Interferon regulatory factor 2 protects mice from lethal viral neuroinvasion

Melody M.H. Li,[1] Leonia Bozzacco,[1] Hans-Heinrich Hoffmann,[1] Gaëlle Breton,[2] Jakob Loschko,[2] Jing W. Xiao,[1] Sébastien Monette,[3] Charles M. Rice,[1] and Margaret R. MacDonald[1]

[1]Laboratory of Virology and Infectious Disease and [2]Laboratory of Molecular Immunology, The Rockefeller University, New York, NY 10065
[3]Tri-Institutional Laboratory of Comparative Pathology, Memorial Sloan-Kettering Cancer Center, The Rockefeller University, Weill Cornell Medical College, New York, NY 10065

The host responds to virus infection by activating type I interferon (IFN) signaling leading to expression of IFN-stimulated genes (ISGs). Dysregulation of the IFN response results in inflammatory diseases and chronic infections. In this study, we demonstrate that IFN regulatory factor 2 (IRF2), an ISG and a negative regulator of IFN signaling, influences alphavirus neuroinvasion and pathogenesis. A Sindbis virus strain that in wild-type (WT) mice only causes disease when injected into the brain leads to lethal encephalitis in *Irf2*$^{-/-}$ mice after peripheral inoculation. *Irf2*$^{-/-}$ mice fail to control virus replication and recruit immune infiltrates into the brain. Reduced B cells and virus-specific IgG are observed in the *Irf2*$^{-/-}$ mouse brains despite the presence of peripheral neutralizing antibodies, suggesting a defect in B cell trafficking to the central nervous system (CNS). B cell–deficient µMT mice are significantly more susceptible to viral infection, yet WT B cells and serum are unable to rescue the *Irf2*$^{-/-}$ mice. Collectively, our data demonstrate that proper localization of B cells and local production of antibodies in the CNS are required for protection. The work advances our understanding of host mechanisms that affect viral neuroinvasion and their contribution to immunity against CNS infections.

INTRODUCTION

During viral infection, recognition of pathogen-associated molecular patterns activates transcription factors IFN regulatory factor 3/7 (IRF3/7) and NF-κB, leading to cytokine and IFN-α/β gene expression (Honda and Taniguchi, 2006; Brennan and Bowie, 2010). IFNs signal through the JAK/STAT pathway and induce downstream expression of antiviral IFN-stimulated genes (ISGs). In addition to modulating the immune response, IFN-α/β is important for immune cell development (Li et al., 2011; Guan et al., 2014; Haynes et al., 2015). Dysregulation of IFN signaling can cause a wide range of disorders and chronic viral infections. Neutralization of type I IFN signaling during persistent lymphocytic choriomeningitis virus (LCMV) infection reduces immune system activation, restores lymphoid architecture, and allows for viral clearance (Teijaro et al., 2013; Wilson et al., 2013). Moreover, type I IFN receptor blockade prevents lethal vascular leakage in susceptible mice in an LCMV model of Lassa fever virus (Baccala et al., 2014). It is not clear how the immune system balances the beneficial and detrimental effects of IFN signaling and how that affects viral infection outcomes. In our study, the role of IRF2, a type I IFN regulator, in alphavirus neuroinvasion and pathogenesis is investigated.

IRF2 is an ISG product that negatively regulates type I IFN production and signaling. IRF2 suppresses the activity of IRF1, a positive regulator of IFN signaling, by competing for binding sites within the promoters of IFN genes and ISGs and potentially limiting the IFN response (Harada et al., 1989). Fibroblasts and peritoneal macrophages from *IRF2* knockout (*Irf2*$^{-/-}$) mice show increased type I IFN mRNA levels upon Newcastle disease virus infection (Matsuyama et al., 1993). *Irf2*$^{-/-}$ mice develop a CD8^{+} T cell–mediated inflammatory skin disease accompanied by ISG up-regulation (Hida et al., 2000; Taki, 2002). Knockout of genes that positively regulate IFN-α/β signaling, such as *IFNAR1* that encodes one subunit of the IFN-α/β receptor or *IRF9*, abolishes disease development in *Irf2*$^{-/-}$ mice, indicating a critical regulatory role for IRF2 in dampening IFN signaling (Hida et al., 2000; Taki, 2002). In addition, IRF2 is important for the development and function of numerous immune cell types including DCs, NK cells, lymphocytes such as T and B cells, and hematopoietic stem cells (Matsuyama et al., 1993; Salkowski et al., 1996; Hida et al., 2000; Lohoff et al., 2000; Honda et al., 2004; Ichikawa et al., 2004; Taki et al., 2005; Sato et al., 2009; Minamino et al., 2012). However, no studies have investigated the maturation and

Correspondence to Margaret R. MacDonald: macdonm@rockefeller.edu

Abbreviations used: BBB, blood–brain barrier; cDC, classical DC; CNS, central nervous system; CT, threshold cycle; DAB, 3,3′-Diaminobenzidine; H&E, hematoxylin and eosin; HIER, heat-induced epitope retrieval; IRF, IFN regulatory factor; ISG, IFN-stimulated gene; LCMV, lymphocytic choriomeningitis virus; MNP, mononuclear phagocyte; p.i., postinfection; PRNT, plaque reduction neutralization test; RT-qPCR, quantitative RT-PCR; SINV, Sindbis virus; TUNEL, terminal deoxynucleotidyl transferase deoxyuridine triphosphate nick-end labeling; VSV, vesicular stomatitis virus.

The Rockefeller University Press $30.00
J. Exp. Med. 2016 Vol. 213 No. 13 2931–2947
https://doi.org/10.1084/jem.20160303

function of immune cell types in *Irf2*$^{-/-}$ mice during the course of a viral infection.

Studies done in the setting of IRF2 overexpression or deficiency demonstrate an antiviral role for this factor. IRF2 exhibits inhibitory effects against several viruses in ISG overexpression screens and synergizes with zinc finger antiviral protein, another ISG, to block Sindbis virus (SINV) replication (Schoggins et al., 2011, 2014; Karki et al., 2012). *Irf2*$^{-/-}$ mice succumb to acute infection with LCMV (Matsuyama et al., 1993). Despite vaccination with an attenuated strain 1 d earlier, *Irf2*$^{-/-}$ mice are susceptible to virulent Venezuelan equine encephalitis virus infection, suggesting IRF2 is required to mount a protective immune response (Grieder and Vogel, 1999). In humans, *IRF2* variants are risk alleles for atopic dermatitis and eczema herpeticum, and some of these single-nucleotide polymorphisms are significantly associated with reduced IFN-γ production after stimulation with herpes simplex virus (Gao et al., 2012). Together, these data support a model in which IRF2 deficiency might lead to increased susceptibility to viral infection.

The *Alphavirus* genus (Togaviridae family) consists of arthropod-borne positive-sense RNA viruses that cause mild to severe disease in humans and animals. Alphaviruses are found worldwide; the Old World viruses, such as SINV and chikungunya virus, cause fever, arthritis, and rash, whereas the New World viruses, such as Venezuelan equine encephalitis virus, can cause encephalitis. SINV, the well-characterized prototype alphavirus, provides a facile model system for studying encephalitis in vivo. Pathogenesis of SINV greatly depends on the virus strain used, route of infection, and the age and genetic background of the mice (Lustig et al., 1988; Sherman and Griffin, 1990; Klimstra et al., 1999; Ryman et al., 2000, 2007; Ryman and Klimstra, 2008). Different SINV strains exhibit different abilities to infect the central nervous system (CNS) and cause disease. Some SINV strains are both neurovirulent (replicate in the brain to cause disease) and neuroinvasive (can invade the CNS and cause disease even after peripheral inoculation), whereas others are neurovirulent but noninvasive and cause encephalitis only when directly inoculated into the brain.

Although mechanisms underlying SINV pathogenesis have been extensively studied, the role of host factors, which modulate viral neuroinvasion after peripheral inoculation in mice with an intact blood–brain barrier (BBB) and a mature immune system, has not been fully explored. Here, we found that IRF2 deficiency confers lethal neuroinvasion on a normally noninvasive SINV strain. We performed detailed virological, histological, and immunological studies to fully characterize the host response to SINV. Our data suggest that defects in multiple immune cell types likely contribute to altered B cell trafficking and pathogenic phenotype in the *Irf2*$^{-/-}$ mice and highlight the important role of IRF2 in the development of the immune system.

RESULTS

IRF2 protects mice from lethal viral neuroinvasion

To study IRF2's antiviral effects on SINV replication in vivo, *Irf2*$^{-/-}$ and WT mice were challenged i.p. with SVN, a neurovirulent but noninvasive strain, which normally replicates only in the periphery without lethality in mice (Lustig et al., 1992). Clinical score, weight loss, and survival of the animals were monitored daily as previously described (Gardner et al., 2008). Approximately 70% of the *Irf2*$^{-/-}$ mice succumbed to infection with SVN, whereas all of the WT littermate control mice survived (Fig. 1 A), indicating that IRF2 deficiency confers lethal neuroinvasive properties on the normally noninvasive SVN strain. Although early disease symptoms were similar in the WT and *Irf2*$^{-/-}$ mice, the disease rapidly progressed in the *Irf2*$^{-/-}$ animals (Fig. 1 B). At early times (days 1 and 2) after i.p. infection, low virus titers were detected in the brains of similar numbers of WT and *Irf2*$^{-/-}$ mice (Fig. 1 C). However, on day 3, virus was not detected in any of the WT mice yet was detected in the brains of all the *Irf2*$^{-/-}$ mice. At later times, the majority of *Irf2*$^{-/-}$ mice had high brain viral titers up to 10^8 PFU/g, whereas an occasional WT animal also had significant viral replication in the brain. These results clearly suggested a failure to clear virus in the brains of the *Irf2*$^{-/-}$ mice. When virus replication in the periphery was monitored, both WT and *Irf2*$^{-/-}$ mice had similar titers in the serum, which was cleared with similar kinetics, but the *Irf2*$^{-/-}$ mice demonstrated prolonged virus replication in the liver and spleen (Fig. 1 C). The difference in viral replication in the brain and the effect of IRF2 on the infection outcome were not caused by a difference in the ability of the virus to replicate in neuronal tissue, as direct inoculation of SVN into the brains was uniformly lethal for both WT and *Irf2*$^{-/-}$ mice (Fig. 1 D). To determine whether IRF2 also protects mice from other neurotropic viruses, *Irf2*$^{-/-}$ and WT littermate control mice were challenged by i.p. injection with vesicular stomatitis virus (VSV). VSV is known to replicate efficiently in the brain and spinal cord and cause acute encephalitis and death in mice by intranasal injection but is highly attenuated and results in no apparent disease after i.p. inoculation (Hastie et al., 2013). Infection with VSV led to survival of all the WT mice, whereas ∼60% of the *Irf2*$^{-/-}$ mice suffered from paralysis and succumbed to infection (Fig. 1 E). Together, these data suggest that IRF2 prevents lethal neuroinvasion of a variety of disparate neurotropic viruses that normally would not efficiently replicate in the CNS after infection through a peripheral route.

Massive neuronal death in *Irf2*$^{-/-}$ mouse brains is not accompanied by immune infiltration

Because the hind limb weakness observed in the WT mice never developed into full-blown paralysis and death (Fig. 1 B), we were interested in identifying differences in the virus-induced CNS damage and the host inflammatory response in SVN-infected WT and *Irf2*$^{-/-}$ animals. We did not detect any sign of pathological changes in the brains of

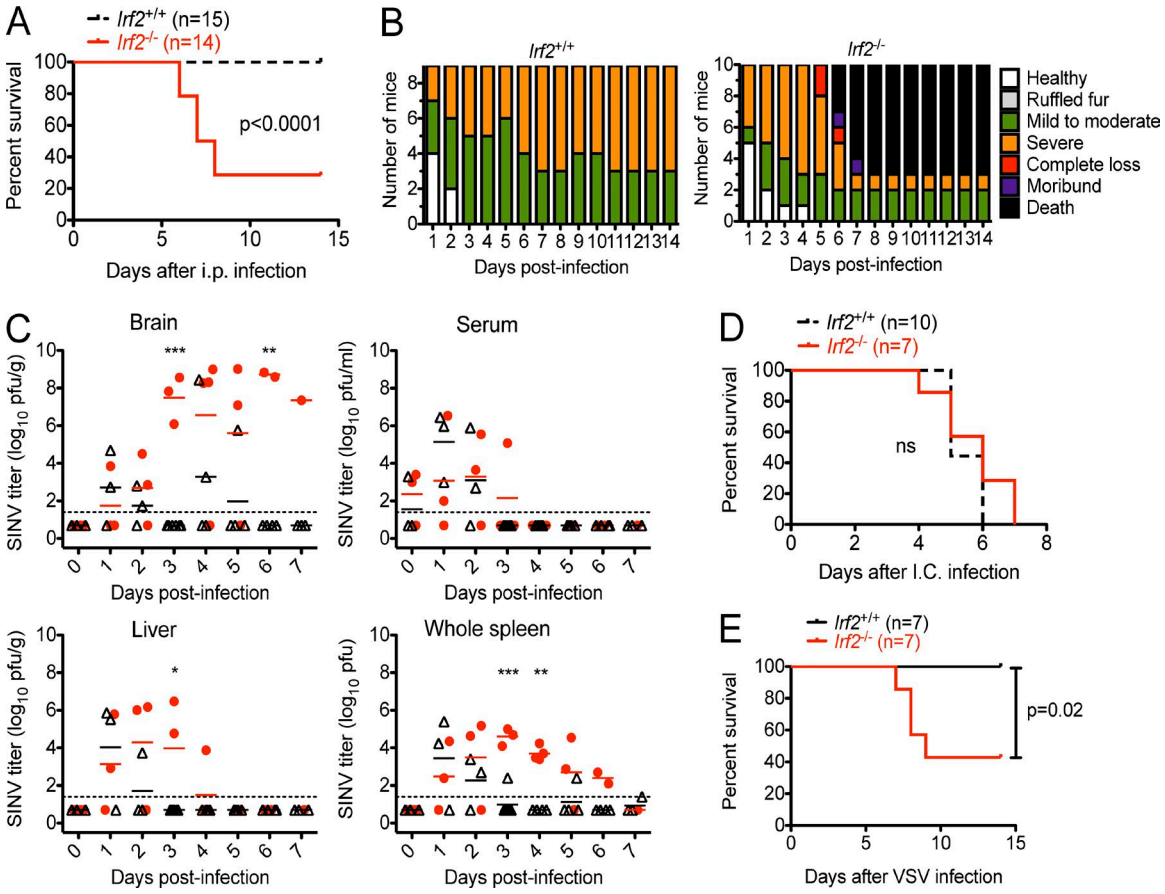

Figure 1. **IRF2 prevents lethal neuroinvasion of disparate neurotropic viruses.** (A and B) Mortality (A) and disease progression (B) of mice infected i.p. with 13,000 PFU SVN were monitored for 14 d. For mortality, a total of 14–15 mice per genotype were infected, divided among seven independent experiments. For measuring clinical symptoms, 9–10 mice per genotype were scored each day. The p-value for the survival curve was determined by the log-rank test ($P < 0.0001$). (C) Viral titers in various tissues of mice infected i.p. with SVN were measured on days 0–7 p.i. Brain, serum, liver, and whole spleens from three to six mice per genotype per time point were harvested and/or homogenized for infection of BHK-21 cells in plaque assays. The dashed line indicates the plaque assay detection limit. Lines represent the mean. Two-way ANOVA test: brain, $P < 0.0001$; whole spleen, $P < 0.001$. Bonferroni posttests: *, $P < 0.05$; **, $P < 0.01$; ***, $P < 0.001$. (D) Mortality of mice infected intracranially (I.C.) with 13,000 PFU SVN was monitored for 7 d. A total of 7–10 mice per genotype were infected, divided among four independent experiments. The p-value for the survival curve was determined by the log-rank test. (E) Mortality of mice infected i.p. with 10,000 PFU VSV was monitored for 14 d. A total of seven mice per genotype were infected in four independent experiments. The p-value for the survival curve was determined by the log-rank test ($P = 0.02$).

the WT and *Irf2*$^{-/-}$ mice on day 1 postinfection (p.i.) when their viral titers were similar. Therefore, we performed histological characterization of various organs of infected WT littermate controls and moribund *Irf2*$^{-/-}$ mice on days 6–7 p.i. WT mouse brains did not exhibit any evidence of pathological changes when stained with hematoxylin and eosin (H&E; Fig. 2 A, left). In contrast, neurons were shrunken, angular, and hypereosinophilic (consistent with neuronal cell death), and the neuropil was vacuolated in both the hippocampus and diencephalon of the *Irf2*$^{-/-}$ mice (Fig. 2 A, middle). The extensive neuronal death was consistent with the known tropism of SINV to replicate mainly in the neurons of the CNS (Jackson et al., 1987, 1988; Sherman and Griffin, 1990). Next, we looked for accumulation of lymphocytes and plasma cells around blood vessels, which was minimal in the brains of both SVN-infected WT and moribund *Irf2*$^{-/-}$ mice (Fig. 2 B, left and middle). Terminal deoxynucleotidyl transferase deoxyuridine triphosphate nick-end labeling (TUNEL) stain, which detects DNA fragmentation in both apoptotic and necrotic cells, was undetectable in WT mouse brains, whereas foci of staining, mostly in the hippocampus, were characteristic of moribund *Irf2*$^{-/-}$ mouse brains (Fig. 2 C, left and middle). In addition, mild myocardial calcification was evident in some *Irf2*$^{-/-}$ mice but was never observed in WT mice. Cytoplasmic viral capsid staining of heart muscle cells was observed in one of these *Irf2*$^{-/-}$ animals, suggesting the heart lesions might be caused by viral replication. Our finding was consistent with previous studies that identified virus replication and associated tissue damage in the hearts of SINV-infected neonatal mice (Trgovcich et al., 1996; Klimstra et al., 1999). The

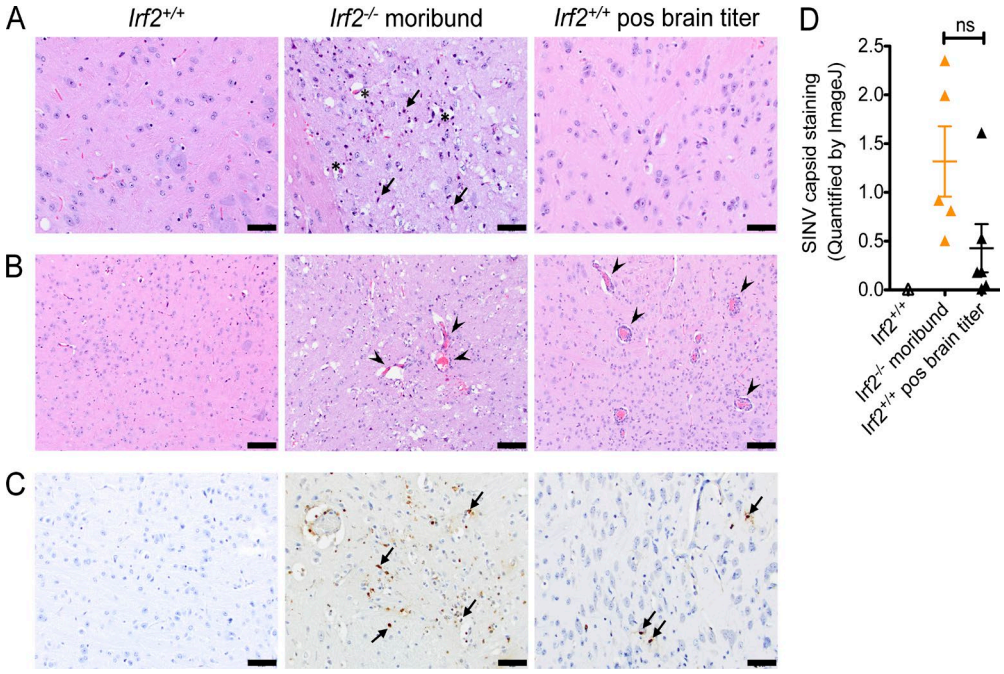

Figure 2. **Extensive neuronal death is observed only in the brains of *Irf2*$^{-/-}$ mice but not in those of WT mice with high viral titers.** (A–C) Representative brain images of three SVN-infected mice from three different groups that demonstrate differences in neuronal morphology (A), perivascular cuffing (B), and neuronal cell death by TUNEL staining (C) are shown. Sections of brain from five SVN-infected WT littermate control mice (left; one animal), five moribund *Irf2*$^{-/-}$ mice (middle; one animal), and six WT mice with high CNS viral titers (right; one animal) were stained with H&E and examined for neuronal cell death (arrows), neuropil vacuolation (asterisks; A), and perivascular cuffing (arrowheads) by morphology (B). (C) TUNEL staining of slides further confirmed the presence of dead cells (brown; arrows). Bars: (A and C) 50 µm; (B) 100 µm. (D) SINV capsid staining of brain slides from the same mice including those with high CNS viral titers was quantified by ImageJ. A sagittal section of the entire brain near the midline was used for viral antigen staining. The p-value was determined by the unpaired, two-tailed Student's *t* test. pos, positive.

histological findings demonstrate extensive neuronal death and tissue damage unaccompanied by immune infiltration in SVN-infected *Irf2*$^{-/-}$ mice. However, the WT mice lack signs of CNS destruction and encephalitis, with no noticeable inflammatory infiltrate, which is likely caused by the absence of viral replication in the brains of these animals late in infection.

Despite a rare event, high brain viral titers were detected in two WT mice on days 4–5 p.i. (Fig. 1 C), allowing us to ask whether there were differential host responses in *Irf2*$^{-/-}$ versus WT animals in the presence of similar levels of viral replication in the CNS. SVN-infected WT mice were euthanized, and their brains were harvested. Five WT mice were identified to have a substantial viral RNA copy number (8.4×10^3 to 2×10^7 copies/µg total brain RNA), and the brains from these mice were processed for histological examination. There was minimal neuronal shrinkage and death in the brains of these WT animals with positive brain viral titers (Fig. 2 A, right). However, compared with *Irf2*$^{-/-}$ animals, significantly more immune cell infiltration was observed on day 5 p.i., characterized by a perivascular cuffing pattern (Fig. 2 B, right). Perivascular cuffing is indicative of an inflammatory response associated with a favorable disease outcome in a previous study that investigated the age-dependent susceptibility of mice to fatal SINV infection (Trgovcich et al., 1999). Only a few isolated cells were marked by the TUNEL stain (Fig. 2 C, right). Quantification of viral capsid staining of whole-brain sections confirmed that these WT mice had viral replication in their brains that was not significantly lower than that in the brains of moribund *Irf2*$^{-/-}$ mice (Fig. 2 D). Altogether, these data show that *Irf2*$^{-/-}$ animals are unable to mount a protective inflammatory response including recruitment of immune cells, which correlates with massive neuronal death and CNS damage not seen in the WT mice with positive brain titers.

Blockade of type I IFN signaling fails to rescue *Irf2*$^{-/-}$ mice

Given IRF2's known role in negatively regulating type I IFN signaling, we measured IFN-α in the serum of WT and *Irf2*$^{-/-}$ mice after i.p. infection with SVN. In WT mice, IFN-α production peaked on day 1 p.i. and waned to undetectable levels by day 3 p.i.; however, in *Irf2*$^{-/-}$ mice, the IFN-α level persisted during the course of the infection and was significantly higher than that in WT animals on days 3 and 6 p.i. (Fig. 3 A). Next, we asked whether this persistent IFN signaling in *Irf2*$^{-/-}$ mice led to up-regulation of inflammatory cytokines. Although the level of monocyte chemotactic protein 1 (MCP-1) was mostly undetectable (5–40 pg/ml serum) and that of IL-6 was comparable (200–900 pg/ml serum) in the serum of WT and *Irf2*$^{-/-}$ mice, they were

significantly up-regulated in *Irf2*$^{-/-}$ mouse brains by day 5 p.i. (Fig. 3 B). We hypothesized that IRF2 deficiency might lead to production of cytokines that damaged the BBB, resulting in uncontrolled viral replication. To measure the BBB integrity, we injected Evans blue, a dye that is normally excluded from the CNS, into the SVN-infected WT and *Irf2*$^{-/-}$ mice by i.p. route on day 2 (when low levels of virus were detectable in the mouse brains of both genotypes), day 3 (when the virus was cleared in WT mouse brains but replicating to high levels in *Irf2*$^{-/-}$ mouse brains), and day 5 (a day before when *Irf2*$^{-/-}$ mice started dying) p.i. On days 2 and 3 p.i., Evans blue entry into the brains of WT and *Irf2*$^{-/-}$ mice, as assessed by fluorescence intensity of brain homogenates, was comparable with that of uninfected mice (Fig. 3 C). By day 5 p.i., accumulation of dye was detected in some of the *Irf2*$^{-/-}$ animals, although the mean fluorescence intensities of WT and *Irf2*$^{-/-}$ mouse brains were not significantly different. The data show that BBB permeability changes are likely not the cause for uncontrolled viral replication but, rather, a result of the massive viral replication and disease in *Irf2*$^{-/-}$ brains during infection.

Next, we measured the mRNA levels of representative ISGs with different roles in IFN signaling. *IFITM3*, *BST2*, *IFIT1*, and *MX1* encode antiviral effectors whereas *OAS1B*, protein kinase R (*PKR*), and *IRF1* gene products are positive regulators of IFN signaling (Schneider et al., 2014). We found higher expression of all the ISGs tested in the brains of *Irf2*$^{-/-}$ mice on days 3 and 5 p.i. (Fig. 3 D). However, WT mice with high brain viral titers (the same mice studied in Fig. 2 D) also expressed enhanced levels of these ISGs on day 5 p.i. (Fig. 3 D), suggesting that expression of ISGs in the brain is induced by SVN replication and not specific to the *Irf2* genotype of the mice. We hypothesized that peripheral elevated type I IFN signaling in *Irf2*$^{-/-}$ animals might contribute to accelerated disease in the CNS. To address this, we injected *Irf2*$^{-/-}$ mice i.p. with IFNAR1-neutralizing antibody before or after infection with SVN to determine whether blockade of type I IFN signaling could rescue *Irf2*$^{-/-}$ mice from lethal neuroinvasion. The WT mice were also treated with IFNAR1-neutralizing antibody before or after infection with SVN as a control. We found that the survival of the *Irf2*$^{-/-}$ mice treated with IFNAR1-blocking antibody 1 d before SVN infection was significantly compromised (Fig. 3 E, left), which, similar to a previous study (Ryman et al., 2000), showed that IFN signaling plays a protective role upon viral challenge. However, the survival of *Irf2*$^{-/-}$ mice treated with IFNAR1-blocking antibody 2 d p.i. was very similar to that of *Irf2*$^{-/-}$ mice treated with an isotype control antibody, suggesting that the protective effects of IFN likely take place early during infection (Fig. 3 E, left). Consistent with the findings of the *Irf2*$^{-/-}$ animals, the survival of the WT mice treated with various amounts of IFNAR1-blocking antibody was compromised, although up to 1 mg was required to significantly decrease the survival of the WT animals (Fig. 3 E, right). Our results suggest that peripheral elevated type I IFN signaling during infection is not responsible for the increased pathology associated with IRF2 deficiency, as neutralization of IFN results in even more severe disease. Given the known role of IRF2 in negative regulation of type I IFN at baseline, we investigated the possibility that dysregulation of the IFN response during the development of the immune system might account for the *Irf2*$^{-/-}$ phenotype.

IRF2 is indispensable for the development and functional maturation of multiple immune cell types at baseline and upon viral challenge

To investigate the importance of IRF2 in the development and maturation of the immune system, we conducted a phenotypic assessment of the major cell types present in the mouse spleen at baseline and during SVN infection on days 1–2 and 5 d p.i., which allowed us to characterize the immune response in the periphery before viral clearance in WT mouse brains and before when *Irf2*$^{-/-}$ mice started dying, respectively. Bulk splenocytes from uninfected and SVN-infected WT and *Irf2*$^{-/-}$ mice were stained for flow cytometric analyses with antibodies specific for T cell, B cell, granulocyte, macrophage, DC, monocyte, and NK cell surface markers (see Fig. S1 for gating strategy). The frequency of splenic NK cells was significantly lower in *Irf2*$^{-/-}$ mice than that in WT mice at baseline (Fig. 4 A). Depending on the time of analysis, lower percentages of B cells, monocytes, and NK cells were present but a higher percentage of granulocytes was detected in *Irf2*$^{-/-}$ mice after infection (Fig. 4 A). Further analyses of specific immune cell subsets revealed that the proportions of $CD4^+$ and $CD8^+$ T cells were significantly different (more $CD4^+$ and less $CD8^+$ T cells) in *Irf2*$^{-/-}$ mice compared with WT mice on days 1 and 5 p.i. (Fig. 4 B). The frequencies of $CD8^+$ and $CD11b^+$ classical DCs (cDCs) were significantly altered at baseline and on days 1, 2, and 5 p.i. in *Irf2*$^{-/-}$ mice (Fig. 4 C). In addition, NK cells in different developmental stages as described in a previous study (Chiossone et al., 2009) were identified and quantified. During infection, percentages of the immature $CD11b^{lo}CD27^{lo}$ and $CD11b^{lo}CD27^{hi}$ NK subsets progressively dropped in the WT mice, likely to give rise to the more mature $CD11b^{hi}CD27^{hi}$ and $CD11b^{hi}CD27^{lo}$ subsets, which steadily increased (Fig. 4 D). On the contrary, the more mature $CD11b^{hi}CD27^{hi}$ and $CD11b^{hi}CD27^{lo}$ NK cells were significantly decreased in *Irf2*$^{-/-}$ mouse spleens, whereas the immature $CD11b^{lo}CD27^{lo}$ and $CD11b^{lo}CD27^{hi}$ cells were more pronounced (Fig. 4 D). Significant differences were observed in the frequencies of the following NK subsets between WT and *Irf2*$^{-/-}$ mice: $CD11b^{hi}CD27^{lo}$ on day 1 p.i. ($P < 0.001$), at baseline, and on days 2 and 5 p.i. ($P < 0.0001$); $CD11b^{hi}CD27^{hi}$ at baseline ($P < 0.01$), on days 1 and 5 p.i. ($P < 0.001$), and on day 2 p.i. ($P < 0.0001$); $CD11b^{lo}CD27^{hi}$ on days 1, 2, and 5 p.i. ($P < 0.0001$); and $CD11b^{lo}CD27^{lo}$ at baseline and on days 2 and 5 p.i. ($P < 0.0001$). Moreover, we investigated two subsets of the $CD115^+$ $CD11b^+$ monocyte population: $Ly6C^{lo}$ patrolling monocytes and $Ly6C^{hi}$ proinflammatory mono-

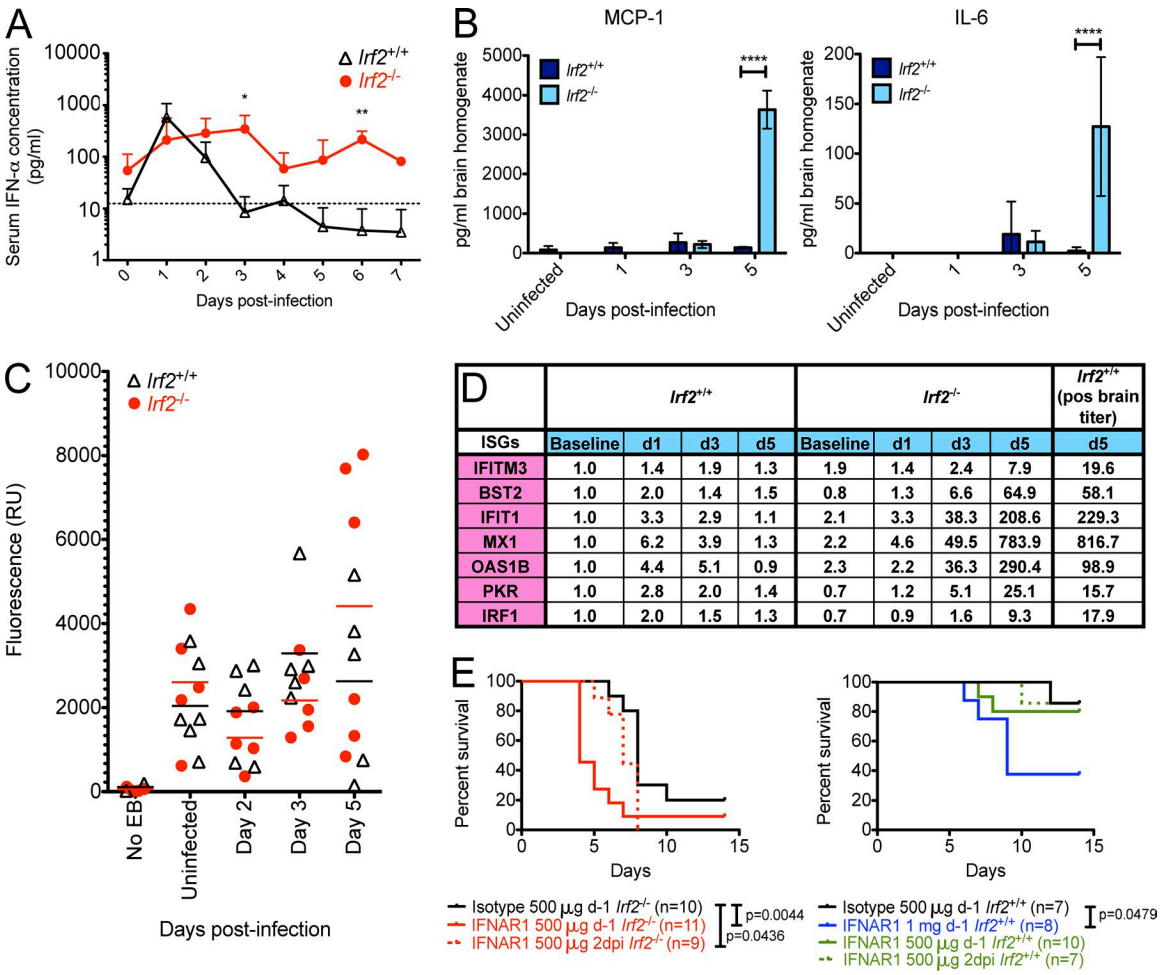

D	Irf2+/+				Irf2-/-				Irf2+/+ (pos brain titer)
ISGs	Baseline	d1	d3	d5	Baseline	d1	d3	d5	d5
IFITM3	1.0	1.4	1.9	1.3	1.9	1.4	2.4	7.9	19.6
BST2	1.0	2.0	1.4	1.5	0.8	1.3	6.6	64.9	58.1
IFIT1	1.0	3.3	2.9	1.1	2.1	3.3	38.3	208.6	229.3
MX1	1.0	6.2	3.9	1.3	2.2	4.6	49.5	783.9	816.7
OAS1B	1.0	4.4	5.1	0.9	2.3	2.2	36.3	290.4	98.9
PKR	1.0	2.8	2.0	1.4	0.7	1.2	5.1	25.1	15.7
IRF1	1.0	2.0	1.5	1.3	0.7	0.9	1.6	9.3	17.9

Figure 3. **Dysregulation of type I IFN signaling during SVN infection is not the cause of accelerated disease and death in *Irf2*$^{-/-}$ mice.** (A) Serum IFN-α levels in WT and *Irf2*$^{-/-}$ mice on days 0–7 p.i. were measured by ELISA during SVN infection. Between three and six infected mice per genotype per time point were tested. Because 70% of the *Irf2*$^{-/-}$ mice succumbed to SVN infection between days 6 and 8 p.i., serum samples from less than three mice were tested on days 6 and 7 p.i. The dotted line indicates the detection limit of the ELISA (concentration of the lowest standard), and error bars represent SD. P-values were determined by the unpaired, two-tailed Student's *t* test. *, P = 0.0167; **, P = 0.0073. (B) Protein concentrations of MCP-1 and IL-6 were measured by cytometric bead array. The right halves of the brains from three to four mice per genotype at baseline or on days 1, 3, and 5 p.i. were harvested and homogenized for measurement of inflammatory cytokines. Error bars represent SD. Two-way ANOVA test: MCP-1, P < 0.0001; IL-6, P < 0.05. Bonferroni posttests: ****, P < 0.0001. (C) Mice were infected i.p. with SVN and injected i.p. with Evans blue (EB) dye to measure BBB permeability on day 2, 3, or 5 p.i. Evans blue cannot cross the BBB unless there is a breach. Brains were harvested and homogenized 3 h after dye injection, and fluorescence present in the homogenates was measured spectrophotometrically. Between five and six mice per genotype served as uninfected controls or were infected, injected with the dye at various time points p.i., and harvested in a total of 11 independent experiments. Between two and four SVN-infected mice per genotype were not injected with the dye but instead harvested for measurement of background fluorescence. RU, relative units. (D) mRNA levels of the indicated ISGs in the brains of WT and *Irf2*$^{-/-}$ mice were measured by RT-qPCR. The right halves of the brains from three to four mice per genotype at baseline or on days 1, 3, and 5 p.i. were harvested and homogenized for RNA extraction. ISG mRNA levels present in the brains of the five WT mice with high CNS viral titers (Fig. 2 D) were also determined. Fold-changes normalized to baseline WT mice for all ISGs tested are shown in the table. ISG mRNA fold-changes with significant differences between the WT and *Irf2*$^{-/-}$ mice were determined using a two-way ANOVA test (IFITM3, P < 0.05; IFIT1, P < 0.05) and Bonferroni posttests (IFITM3 on day 5 p.i., P < 0.01; IFIT1 on day 5 p.i., P < 0.01; MX1 on day 5 p.i., P < 0.05; protein kinase R [PKR] on day 5 p.i., P < 0.01; IRF1 on day 5 p.i., P < 0.05). pos, positive. (E) Mortality of mice treated with 500 µg or 1 mg IFNAR1-blocking antibody or 500 µg isotype control antibody by i.p. route 1 d before or 2 d after i.p. infection with SVN. A total of 9–11 *Irf2*$^{-/-}$ and 7–10 WT mice were treated with IFNAR1-blocking antibody or isotype control and infected with SVN, divided among nine independent experiments. The p-values for survival curves were determined by the log-rank test. Only the significant differences are shown (isotype vs. IFNAR1 500 µg day −1 *Irf2*$^{-/-}$, P = 0.0044; isotype vs. IFNAR1 500 µg 2 d p.i. *Irf2*$^{-/-}$, P = 0.0436; isotype vs. IFNAR1 1 mg day −1 *Irf2*$^{+/+}$, P = 0.0479).

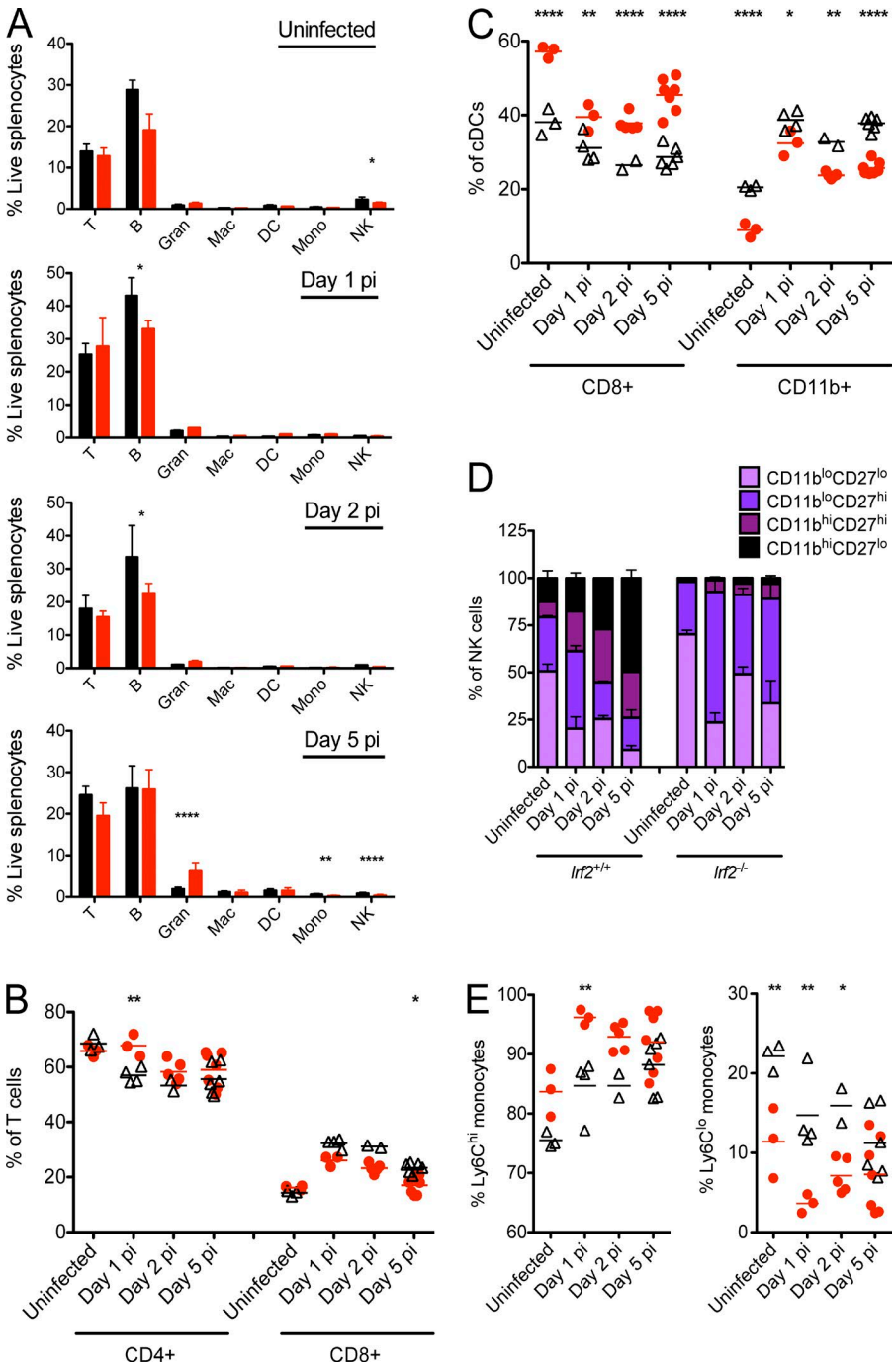

Figure 4. **Development and maturation of multiple immune cell subsets are compromised in *Irf2*$^{-/-}$ mice at baseline and upon SVN infection.** (A) Bulk splenocytes from uninfected and SVN-infected WT and *Irf2*$^{-/-}$ mice on days 1, 2, and 5 p.i. were isolated and stained with antibodies specific for T cell (T), B cell (B), granulocyte (Gran), macrophage (Mac), DC, monocyte (Mono), and NK cell surface markers for flow cytometric analyses (see Fig. S1 for gating strategy). The graphs show frequencies of various immune cell populations as percentages of live splenocytes (black bars, WT; red bars, *Irf2*$^{-/-}$). (B–E) The percentages of CD4$^+$ and CD8$^+$ T cells (B), CD8$^+$ and CD11b$^+$ cDCs (C), NK subsets with increasing maturation indicated by color intensity (D), and Ly6C^{hi} and Ly6C^{lo} monocytes (E) are shown. Black open triangles and red closed circles represent WT and *Irf2*$^{-/-}$ mice, respectively. Spleens from two to seven mice per genotype per time point were analyzed in a total of seven independent experiments. Error bars represent SD. Bonferroni posttests: *, $P < 0.05$; **, $P < 0.01$; ****, $P < 0.0001$.

cytes (Hanna et al., 2011; Shi and Pamer, 2011). We found dramatically lower percentages of Ly6C^{lo} monocytes in *Irf2*$^{-/-}$ mice at baseline and on days 1 and 2 after SVN infection, whereas Ly6C^{hi} monocytes existed at a higher frequency on day 1 p.i. (Fig. 4 E). Our findings clearly highlight the function of IRF2 in maintaining the homeostasis of different immune cell lineages in the spleen.

Because IRF2 deficiency dramatically compromised the frequency and maturation of multiple immune cell types, we took depletion and reconstitution approaches to investigate whether one or several of these affected cell types contributed to lethal SVN neuroinvasion. We focused on NK cells, cDCs, and monocytes because they were most significantly altered by *IRF2* knockout and/or important for SINV infection (Ryman and Klimstra, 2008). First, we depleted the NK cells in the WT mice 1 d before viral infection to probe the protective role of NK cells in SVN pathogenesis. Although our depletion conditions led

to a 95% reduction in the frequency of $CD3^-$ $NK1.1^+$ cells, there was no significant difference in the survival of the WT mice lacking splenic NK cells (Fig. 5 A). Our finding was consistent with a previous study that showed no role for NK cells in protection from SINV (Hirsch, 1981). Mononuclear phagocytes (MNPs) consist of macrophages, monocytes, and DCs and can be depleted with clodronate liposomes. We asked whether removing MNPs, including cDCs and monocytes that were negatively impacted by IRF2 deficiency, affects SINV pathogenesis. If $Irf2^{+/+}$ MNPs are protective, depletion would cause accelerated disease in WT mice. However, if the *Irf2*-null MNPs are detrimental, depletion would ameliorate disease in $Irf2^{-/-}$ mice. We treated WT and $Irf2^{-/-}$ mice with clodronate to deplete MNPs or used PBS liposomes as a control and found no significant difference in the survival of the mice under these two conditions (Fig. 5 B). However, there was large variability among animals in cDC, macrophage, and monocyte depletion by clodronate liposomes. We observed that 93–96% of macrophages (three out of four mice), 36–56% of cDCs (three out of four mice), and 46–58% of $Ly6C^{lo}$ patrolling monocytes (four out of four mice) were depleted, whereas $Ly6C^{hi}$ proinflammatory monocytes were unaffected (four out of four mice). Given the age and size of the animals, we were unable to use tail vein administration, which is known to be more efficient at phagocytic depletion. All in all, these data suggest that none of the cell types that were removed from WT or $Irf2^{-/-}$ mice are sufficient to reverse the phenotype. IRF2 likely creates a supportive environment for the proliferation and maturation of multiple immune cell subsets that together protect mice from lethal neuroinvasion.

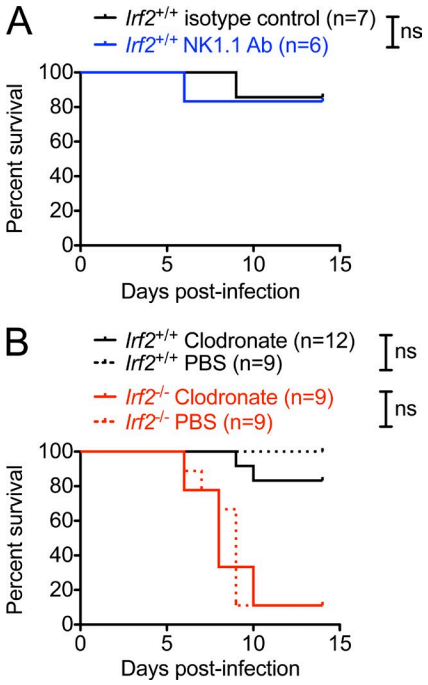

Figure 5. **Depletion of NK cells or MNPs does not significantly alter viral pathogenesis.** (A) Mortality of WT mice treated i.p. with 300 µg NK1.1 antibody (Ab) or an isotype control 1 d before i.p. infection with SVN was monitored. A total of six to seven WT mice were treated and infected, divided between two independent experiments. (B) Mortality of WT and $Irf2^{-/-}$ mice treated i.p. with 200 µl clodronate or PBS liposomes 3 d before i.p. infection with SVN was monitored. A total of 9–12 mice per genotype were treated and infected, divided among eight independent experiments. The p-values for survival curves were determined by the log-rank test.

B cell number and virus-specific IgG level are significantly lower in $Irf2^{-/-}$ mouse brains

A major difference in the host response to SVN infection between moribund $Irf2^{-/-}$ mice and the few littermate control WT mice with high viral brain titers was immune infiltration (Fig. 2 B, middle and right). We next asked whether higher numbers of one or multiple immune cell types were observed in WT mouse brains. Adjacent sections from the brains of SVN-infected $Irf2^{-/-}$ and WT mice with high CNS viral titers (Fig. 2 D) were stained with antibodies specific for T cells, B cells, granzyme-containing cells (cytotoxic $CD8^+$ T and NK cells), and macrophages. Each was examined and scored semiquantitatively for the frequency of positively stained cells. The brains of WT mice had a higher number of B cells compared with those of the $Irf2^{-/-}$ mice, whereas the other cell types existed at similar frequencies among the mice (Fig. 6 A). Images that consistently sampled eight different regions in the brains (Fig. S2) of WT and $Irf2^{-/-}$ mice were used to quantify B cell staining by ImageJ or by manual cell counting. Consistent with the semiquantitative histological scoring (Fig. 6 A), the WT mice with positive viral titers in the brains had a significantly higher number of B cells compared with the moribund $Irf2^{-/-}$ mice (Fig. 6 B). To understand whether the elevated B cell numbers in WT mouse brains correlate with an effective immune response, we measured the levels (Fig. 6 C) and quality (Fig. 6 D) of SVN-specific antibodies in the serum and brains of WT and $Irf2^{-/-}$ mice infected with SVN. Interestingly, although both WT and $Irf2^{-/-}$ mice were able to mount virus-specific antibody responses in the periphery that can effectively neutralize SVN (Fig. 6, C and D), only WT mice had a robust SINV-specific IgG titer in the brain, which occurred on day 7 p.i. (Fig. 6 C). These antibodies could either enter the brain through a breach in the BBB or be produced locally by B cells that have infiltrated the CNS. The latter was more likely because the levels of virus-specific IgG in the periphery were comparable between WT and $Irf2^{-/-}$ animals before day 7 p.i. B cell migration to or proliferation in the $Irf2^{-/-}$ mouse brains was likely deterred, leading to lower numbers of B cells and lower levels of virus-specific IgG in the CNS. Our findings suggest that B cell number in the mouse brains is affected by IRF2 deficiency, which is consistent with the immune defects observed in the periphery.

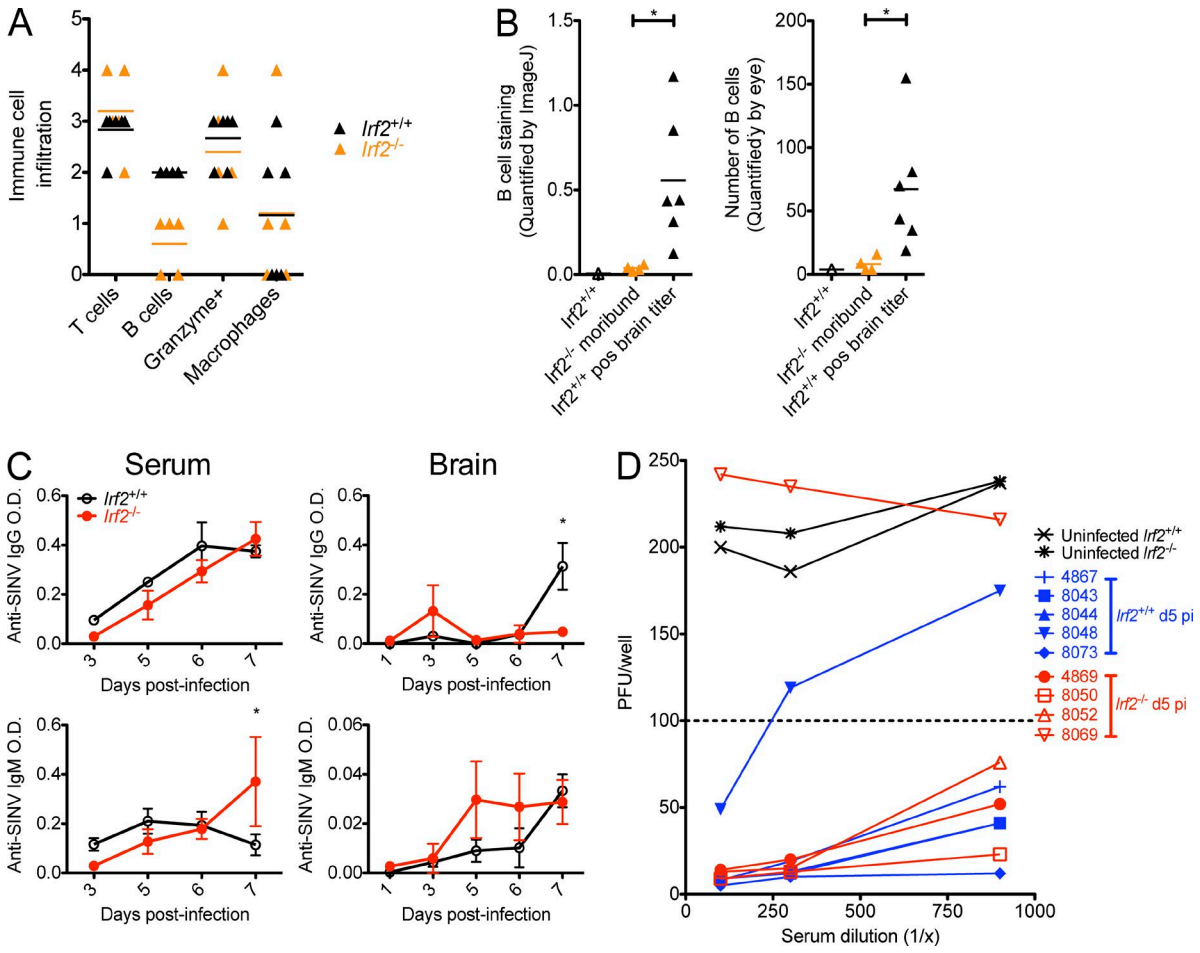

Figure 6. **B cells and virus-specific IgG level are significantly reduced in *Irf2*$^{-/-}$ mouse brains.** (A) Brain slides from five *Irf2*$^{-/-}$ moribund mice and six SVN-infected WT mice with high CNS viral titers from Fig. 2 D were stained with antibodies specific for CD3 (T cell), B220 (B cell), granzyme (cytotoxic T and NK cells), and Mac2 (macrophage). Immune cell infiltrates were semiquantitatively scored using a scale of zero to four as follows: 0, absent; 1, minimal; 2, mild; 3, moderate; and 4, marked. (B) Images that consistently sample eight different regions in the brains (Fig. S2) of WT and *Irf2*$^{-/-}$ mice were taken, and the B cell staining present in those images was quantified by ImageJ (measurement of number of positive pixels) or by eye (number of B cells). The p-values were determined by the unpaired, two-tailed Student's *t* test (*, $P < 0.05$). pos, positive. (C) SINV-specific IgG and IgM antibodies in serum and brain homogenate samples of infected mice were measured by ELISA, as detailed in the ELISA section of Materials and methods. Mean OD value represents the level of virus-specific IgG or IgM antibody. Serum samples from three to six mice (except for $n = 2$ for *Irf2*$^{-/-}$ on day 7 p.i.) and brain homogenates from three mice per genotype per time point were tested for antibody titers. Error bars represent SD. Bonferroni posttests: *, $P < 0.05$. (D) PRNT was performed on serum samples of uninfected ($n = 1$ per genotype) and day 5 SVN-challenged WT and *Irf2*$^{-/-}$ mice ($n = 4$–5 per genotype). Infection with a constant concentration of virus incubated with serum samples from uninfected mice resulted in ~200 plaques per well. The point at which the dilution curve crosses the dotted line represents the concentration of serum from SVN-infected mice required to reduce the number of plaques by 50%.

Proper localization of B cells and antibodies to the CNS is required for protection

To demonstrate that B cells are critical for protection from SVN infection, B cell–deficient μMT mice and age-matched WT C57BL/6J mice were challenged with SVN (Fig. 7 A). We found that μMT mice were significantly more susceptible to SVN-induced paralysis and death, suggesting that B cells are required for protection from lethal neuroinvasion. To test the hypothesis that B cells and a virus-specific antibody response are required in the CNS, we adoptively transferred WT B cells and serum to *Irf2*$^{-/-}$ mice. B cells were isolated from naive WT mice and retroorbitally adoptively transferred to *Irf2*$^{-/-}$ mice (and WT controls) 1 d before infection with SVN (Fig. 7 B). Whereas only one out of eight WT mice succumbed to SVN infection, six out of six *Irf2*$^{-/-}$ mice died by day 9 p.i., suggesting that B cells from naive WT mice are not sufficient to rescue *Irf2*$^{-/-}$ mice from the disease. In addition, serum was harvested from SVN-infected mice on day 7 p.i. and i.p. adoptively transferred to *Irf2*$^{-/-}$ mice (and WT controls) 1 d after infection (Fig. 7 C). Day 7 p.i. was chosen because it was the day when a significant difference in the levels of virus-specific IgG was observed in the brains

but not in the periphery of WT and *Irf2*$^{-/-}$ mice. We found that serum transfer did not protect all *Irf2*$^{-/-}$ mice from lethal neuroinvasion by SVN, although a higher percentage of *Irf2*$^{-/-}$ mice survived compared with those that received no serum (Fig. 1 A). Because we administered the serum to the mice much earlier (1 d p.i.) than when they actually would mount an antibody response (Fig. 6 C), it is possible that the slight protective effect was caused by virus neutralization in the periphery before virus gaining access to the brain. However, overall, our data suggest that antibodies in the periphery fail to adequately protect mice from fatal CNS disease, likely because of the inability of the antibodies to cross the BBB. Collectively, our data suggest that appropriate environmental cues missing in *Irf2*$^{-/-}$ mice are required for B cell trafficking and function, and protection in WT mice is likely conferred by proper localization of B cells and antibodies to the CNS.

DISCUSSION

We reported in this study that IRF2 deficiency confers rapid and lethal neuroinvasion of SVN that is typically cleared from the brains of WT mice. A mosquito isolate of SINV, the SV strain, was serially passaged in suckling and weanling mouse brains to generate SVN (neurovirulent but noninvasive) and SVNI (neurovirulent and invasive; Lustig et al., 1992). Both SVN and SVNI can cause lethal encephalitis after intracranial inoculation, but only SVNI can invade the CNS and cause high levels of replication in the brain upon peripheral infection (Lustig et al., 1992). Intriguingly, the lack of IRF2 converts the phenotype of SVN to that of SVNI. It is possible that IRF2 normally prevents SVN from efficiently entering the CNS by mechanisms similar to those used by SVNI. The determinants for neuroinvasion of SVNI are mapped to three mutations, two of which confer amino acid changes in the E2 glycoprotein, which is important for cellular entry (Dubuisson et al., 1997). A study using packaged SINV replicons demonstrated that mutations in E2 confer the ability to infect human DCs, suggesting that infection of innate immune subsets such as DCs might be critical for SINV neuroinvasion (Gardner et al., 2000). IRF2 deficiency might facilitate more efficient infection of immune cells by SVN, and as a result, the virus spreads to the CNS and causes lethal neuroinvasion in mice.

In addition, our study points to a relationship between IRF2 expression and immune cell development. Frequencies of both total and subset populations of multiple cell types are altered in the spleens of *Irf2*$^{-/-}$ mice. *Irf2*$^{-/-}$ mice have not only fewer NK cells and proportionally less mature cells at baseline, but also reduced expansion of the more mature NK subsets during infection compared with WT animals (Fig. 4, A and D). Because CD11b^{hi}CD27^{hi} and CD11b^{hi}CD27^{lo} NK cells differentiate from CD11b^{lo}CD27^{lo} and/or CD11b^{lo}CD27^{hi} cells and a major difference between CD11b^{lo}CD27^{hi} and CD11b^{hi}CD27^{lo} NK cells is their proliferative potential (Chiossone et al., 2009), it is likely that immature NK cells are defective in proliferation and differentiation into the more mature subsets in *Irf2*$^{-/-}$ mice at baseline and upon viral challenge. IRF2 can affect NK cell development either directly or indirectly by altering the development of other immune cell types required for the development of NK cells. DCs, which were also affected by IRF2 deficiency, have been shown to control NK cell proliferation and effector functions (Lucas et al., 2007; Hochweller et al., 2008). In our study, the frequency of Ly6C^{lo} monocytes was dramatically affected by IRF2 deficiency. At baseline and after infection, *Irf2*$^{-/-}$ mice have a lower frequency of Ly6C^{lo} patrolling monocytes but a higher frequency of Ly6C^{hi} inflammatory monocytes compared

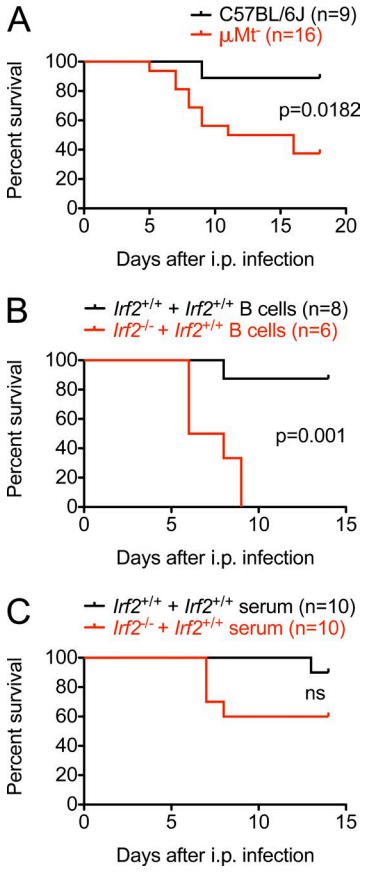

Figure 7. **B cells are protective against lethal viral neuroinvasion.** (A) Mortality of B cell–deficient μMT and age-matched WT C57BL/6J mice infected i.p. with 13,000 PFU SVN was monitored for 18 d. A total of 9–16 mice per genotype were infected, divided between two independent experiments. The p-value for the survival curve was determined by the log-rank test (P = 0.0182). (B) WT and *Irf2*$^{-/-}$ mice with B cells retroorbitally adoptively transferred from WT mice were infected i.p. with 13,000 PFU SVN the day after, and their mortality was monitored for 14 d. A total of six to eight mice per genotype were infected, divided between two independent experiments. The p-value for the survival curve was determined by the log-rank test (P = 0.001). (C) WT and *Irf2*$^{-/-}$ mice were infected i.p. with 13,000 PFU SVN, and 1 d later, serum from infected WT mice (day 7 p.i.) was adoptively transferred to the animals. Their mortality was monitored for 14 d. A total of 10 mice per genotype were infected, divided among five independent experiments. The p-value for the survival curve was determined by the log-rank test.

with WT mice (Fig. 4 E). Our data suggest that differentiation of Ly6C^{lo} monocytes from Ly6C^{hi} ones might be defective in the absence of IRF2, although it is still controversial whether Ly6C^{lo} monocytes differentiate directly from a bone marrow progenitor or from mature Ly6C^{hi} monocytes (Varol et al., 2007; Auffray et al., 2009; Hanna et al., 2011). Future work investigating the developmental stage at which IRF2 acts and whether IRF2 affects the function of these monocyte subsets is warranted.

Among the studies that have identified specific immune cell types negatively impacted by IRF2 deficiency, some demonstrate a link between elevated type I IFN production and/or signaling and immune cell dysfunction. Knocking out IFNAR1 restores the normal phenotype of some affected immune subsets (Hida et al., 2000; Honda et al., 2004; Ichikawa et al., 2004; Sato et al., 2009; Minamino et al., 2012) but not the developmental arrest of NK cells in the bone marrow (Ichikawa et al., 2004), suggesting that IRF2 facilitates the development and maturation of different immune cell types by disparate mechanisms. The involvement of type I IFN in immune cell development and function is further confounded by a recent study demonstrating that NK cells from mice deficient in IFNAR1 or STAT1, which signals downstream of the IFN-α/β receptor, are defective in expansion and memory cell formation after mouse cytomegalovirus infection (Madera et al., 2016). Hence, the contribution of IFN signaling to IRF2-dependent effects on immune cell development might differ before and after viral challenge. IRF2 also positively regulates expression of some genes (Taki, 2002) and therefore can act in an IFN-independent way by transcriptionally regulating diverse host genes important for cell proliferation and activation. A recent study of human monocytes identified a single-nucleotide polymorphism controlling IRF2 expression level in response to LPS and IFN-γ and identified a network of 300 genes differentially regulated by IRF2 levels (Fairfax et al., 2014).

Because NK cells, cDCs, and monocytes are most dramatically affected by IRF2 deficiency, we performed a series of depletion and reconstitution experiments to determine their roles in alphavirus infection and pathogenesis. Even though cells with natural killer activity are found in the cerebrospinal fluid of mice with acute SINV encephalitis (Griffin and Hess, 1986), there are no significant differences in SINV replication and pathogenesis of both footpad and intracerebral infections in NK cell–deficient mice compared with that of NK cell–normal mice (Hirsch, 1981). These data are consistent with our results of NK cell depletion by antibody treatment in WT mice and suggest that NK cells are dispensable for control of SINV infection. However, the role of phagocytic cells including cDCs and monocytes in SINV neuroinvasion is inconclusive given the difficulty of having an ideal depletion system for these populations (Chow et al., 2011). We have found that clodronate treatment is highly variable and inefficient at equally depleting all the cDCs, macrophages, and monocytes. Generation of conditional knockout mice will allow direct interrogation of IRF2 function in the development and response of specific cell types to SINV infection in future studies.

Moreover, we have discovered a B cell defect in *Irf2*$^{-/-}$ mice. Significantly lower numbers of splenic B cells are present in *Irf2*$^{-/-}$ mice on days 1 and 2 p.i. with SVN, suggesting that B cell homing or proliferation might be affected upon viral infection. Consistent with our finding, a previous study demonstrated that B220^{hi}/surface IgM^{+} cells representing newly generated and returning mature B cells exist at lower numbers in the bone marrow of *Irf2*$^{-/-}$ mice (Matsuyama et al., 1993). Serum IgG2a levels in *Irf2*$^{-/-}$ mice are significantly reduced, and both their bone marrow cells and splenocytes are less responsive to LPS and cytokines (Matsuyama et al., 1993). We have also found a significantly lower number of B cells and attenuated IgG response in *Irf2*$^{-/-}$ mouse brains despite similar levels of neutralizing antibodies in the serum of WT and *Irf2*$^{-/-}$ animals (Fig. 6). Because by days 6–7 p.i. none of the infected WT mice have detectable virus in their brains (Fig. 1 C), these findings suggest that B cells and virus-specific antibody responses might contribute to viral clearance and disease resolution in the CNS. In support of that, B cell–deficient μMT mice are significantly more susceptible to lethal neuroinvasion by SVN (Fig. 7 A), which demonstrates a protective role for B cells.

B cells are known to be critical for protection of SINV-infected mice from neuropathology, as antibodies can mediate viral clearance from the CNS by a mechanism that is distinct from classical antibody-dependent cell-mediated cytotoxicity or complement-dependent lysis (Levine et al., 1991). Some of the monoclonal antibodies that recognize major epitopes of SINV E1 and E2 envelope glycoproteins are able to clear the virus from the brain and spinal cord of SINV-infected SCID mice (Levine et al., 1991). Because adoptive transfer of naive B cells and serum from infected WT mice fails to rescue *Irf2*$^{-/-}$ mice from lethal neuroinvasion (Fig. 7, B and C), IRF2 is likely required for the proper localization of B cells and antibodies to the CNS. A recent study using a mouse model of genital herpes infection has defined a requirement for CD4 T cells, specifically memory CD4 T cells, in protection of neuronal tissues after immunization at a distal site (Iijima and Iwasaki, 2016). Memory CD4 T cells secrete IFN-γ to mediate BBB permeability and optimal antibody penetration into the dorsal root ganglia and spinal cord. IRF2 might regulate memory CD4 T cell function or recruitment to the neuronal tissue. Alternatively, IRF2 might be involved in the proper transcriptional control of chemokine and chemokine receptor genes that recruit B cells to sites of SINV infection or promote their proliferation in the CNS. In response to SINV infection, expression of local inflammatory chemokines and cytokines that attract leukocytes into the CNS and facilitate B cell proliferation and differentiation increase rapidly, and surface expression of chemokine receptors is also detected on infiltrating B cells (Metcalf et al., 2013). The exact mechanism of how IRF2 controls B cell and antibody access to the CNS needs to be further investigated.

In conclusion, we have demonstrated a novel function for IRF2 in protecting mice from lethal viral neuroinvasion, which is dependent on the normal development and maturation of the immune compartment and a virus-specific B cell response in the CNS. The recent Zika virus and chikungunya virus outbreaks of unprecedented scale in multiple countries urge the development of antivirals and prophylactic treatments to prevent global spread of emerging viruses that can cause severe disease in the CNS (Schuffenecker et al., 2006; Pialoux et al., 2007; Powers and Logue, 2007). Given type I IFN's clinical applications and potential effects on vaccine efficacy, our study is highly relevant and enhances our understanding of the multifaceted role of IFN regulators in the modulation of immune responses.

MATERIALS AND METHODS

Mice and infections

Irf2$^{+/-}$ mice on a pure C57BL/6J background were obtained from T.W. Mak (University of Toronto, Toronto, Canada; Matsuyama et al., 1993) and maintained and bred at the Comparative Bioscience Center (CBC) of The Rockefeller University to generate *Irf2*$^{-/-}$ pups and WT littermate controls. B cell–deficient μMT (B6.129S2-*Ighm*^{tm1Cgn}/J) and C57BL/6J mice were purchased from The Jackson Laboratory and maintained and bred at the CBC of The Rockefeller University to generate μMT pups and age-matched WT C57BL/6J controls. 24–26-d-old mice of both gender were infected either i.p. or intracranially with 13,000 PFU of the SINV strain, SVN, diluted in PBS. The i.p. lethal dose, 50% for SVN was previously determined to be $>3 \times 10^7$ PFU by i.p. infection of CD-1 mice (Dubuisson et al., 1997). Mice were infected i.p. at 24–26 d old with 10,000 PFU of VSV, San Juan strain (Bick et al., 2003) diluted in PBS. For assessment of morbidity and mortality, mice were monitored daily using the following scoring system: 0, no disease signs; 1, ruffled fur; 2, mild to moderate hind limb weakness; 3, severe hind limb weakness/dragging; 4, complete loss of hind limb function; 5, moribund; and 6, death. For tissue collection, mice were euthanized with CO_2 and exsanguinated via cardiac puncture. Livers, spleens, and brains were collected, weighed, and stored at −80°C. All experiments in mice were performed at the CBC under protocols approved by the Institutional Animal Care and Use Committee at The Rockefeller University.

Virus assays

Virus titers were determined as previously described (Levine et al., 1991). Frozen tissue was homogenized in 500 μl PBS to generate liver, spleen, and brain homogenates that were then clarified by centrifugation. The amount of infectious virus was determined by plaque formation on BHK-21 cells. Because 70% of the *Irf2*$^{-/-}$ mice succumbed to SVN infection between days 6 and 8 p.i., serum samples and tissues from less than three mice were titered on days 6 and 7 p.i. Data were plotted as the mean $\log_{10}$ value of PFU for each animal and the mean of each genotype group per time point p.i. The limit of detection (in $\log_{10}$) for the plaque assay (one plaque detected at 1:10 dilution in one of the duplicate plaque assay wells) is 1.3979. For statistical purposes, samples in which no virus was detected at a 1:10 dilution were assigned a value of 0.7, which is halfway between the limit of detection and zero. Virus titers per milliliter of serum, gram of tissue (brain and liver), or whole spleen were plotted. To determine SVN RNA levels in the brains of infected mice, 500 ng of total RNA extracted from the right halves of the brains was used in a one-step quantitative real-time PCR assay using primers and a TaqMan probe targeting the nsP2 region of SINV. Primer pairs for SINV TaqMan quantitative RT-PCR (RT-qPCR) were obtained from H. Chung (The Rockefeller University, New York, NY) and are listed in Table S1. RNA from mouse brains was amplified using RNA Master Hydrolysis Probes (Lightcycler 480; Roche) under the following thermal conditions: RT at 63°C for 3 min; denaturation at 95°C for 30 s; 45 cycles of amplification at 95°C for 15 s, 60°C for 30 s, and 72°C for 1 s; and a final cooling step at 40°C for 10 s. Viral RNA copy number of a given brain sample was then determined by comparing the threshold cycle (CT) value to a standard curve of serial 10-fold dilutions of purified in vitro transcribed SVN RNA.

BBB permeability

Permeability of the BBB was quantified by Evans blue using standard techniques (Wang et al., 2004; Rhodehouse et al., 2013). *Irf2*$^{-/-}$ mice and WT littermates were injected with Evans blue dye i.p. at 3% in 100 μl of sterile PBS. 3 h later, mice were anesthetized with ketamine/xylazine; blood was collected by cardiac puncture followed by transcardial perfusion to flush the remaining blood from the cerebrovasculature. Brains were rapidly harvested and weighed. Brains were homogenized with magnetic beads in 0.5 ml ice-cold PBS in TissueLyser followed by centrifugation at 15,000 rpm for 5 min at 4°C. Supernatants were used for fluorescence measurements (excitation at 540 nm and emission at 680 nm).

RT-qPCR

The left halves of the brains were homogenized in PBS, and the supernatant was stored in TRIzol at −80°C. Phase separation was performed according to the manufacturer's instructions, followed by RNA isolation with an RNeasy mini kit (QIAGEN). RNA was quantified using a nanodrop spectrophotometer. 1 μg of input RNA was used as a template for RT using SuperScript III (Invitrogen) and random hexamers. RT-qPCR was performed using 5 μl of 10-fold–diluted cDNA in a SYBR green quantitative PCR assay on a real-time PCR system (LightCycler 480; Roche). Primer pairs for RT-qPCR are listed in Table S1. Primers for measuring IFITM3 and BST2 mRNAs were obtained from M. Dittmann (New York University School of Medicine, New York, NY). Expression levels of mouse ISGs were determined by normalizing the target transcript CT value to the CT value of the endogenous

housekeeping RPS11 transcript. This normalized value was used to calculate the fold-change relative to the mean of the baseline WT controls (CT method).

Cytokine and chemokine protein quantification by cytometric bead array

IL-6 and MCP-1 levels in serum and clarified brain homogenates were determined using a cytometric bead array mouse inflammation kit (BD). The right halves of the brains were homogenized in radioimmunoprecipitation assay buffer + protease inhibitor, and the supernatant was stored at −80°C. Serum and clarified brain homogenates diluted 1:5 were used as input samples, and the manufacturer's protocol was followed. The limit of detection was 20 pg/ml of serum or brain homogenate.

ELISA

ELISA was performed to measure SINV-specific antibody (Kulcsar et al., 2015). 96-well Maxisorp plates (Thermo Fisher Scientific) were coated with 10^6 PFU/well of polyethylene glycol–precipitated SINV strain SVN in 0.1 M Na_2CO_3, pH 9.6, at 4°C overnight. Blocking buffer (10% FBS and 0.05% Tween 20 in PBS) was added for 2 h at 37°C. The right halves of the brains were homogenized in radioimmunoprecipitation assay buffer + protease inhibitor, and the supernatant was stored at −80°C. Serum samples diluted 1:10 and brain homogenates diluted 1:2 in blocking buffer were added to the coated plates and incubated at 4°C overnight. Bound antibodies were detected using HRP-conjugated goat anti–mouse IgG (Jackson ImmunoResearch Laboratories, Inc.) or IgM (Sigma-Aldrich) diluted 1:1,000 in blocking buffer and incubated at room temperature for 2 h. Plates were developed using the TMB Liquid Substrate System (Sigma-Aldrich) for ELISA with H_2SO_4 as a stop solution. Absorbance was read at 450 nm in a FLUOstar Omega Plate Reader (BMG Labtech). Mean OD values for serum and brain samples from uninfected WT and *Irf2*$^{-/-}$ mice were subtracted from the OD values of samples from the infected mice.

Measurement of IFN levels

The Verikine Mouse IFN-α ELISA kit (PBL Interferon Source) was used to measure IFN-α levels by following the manufacturer's instructions. The range of detection was 12.5–400 pg IFN-α per ml serum.

Splenocyte isolation

Single-cell suspensions from spleen tissues were prepared as previously described (Schreiber et al., 2013). In brief, whole mouse spleens were mechanically disrupted and incubated with HBSS + 5% FBS + 0.5 mg/ml collagenase (Roche) at 37°C for 30 min. Cells were filtered through 100-µM cell strainers and washed. Red blood cells were removed by incubating the pellet with 1 ml ACK lysing buffer (Gibco) at room temperature for 5 min. Splenocytes were then pelleted and resuspended in HBSS + 5% FBS, and live cells were counted using trypan blue exclusion.

Flow cytometry

Approximately 3×10^6 cells were used for immunophenotyping by flow cytometry. Cells were blocked using rat anti–mouse CD16/CD32 (eBioscience) and stained with antibodies for 30 min at 4°C. Cells were then fixed and resuspended in 150 µl for flow cytometric acquisition. Forward- and side-scatter parameters were used to gate out doublets. The antibodies used were from BD, Thermo Fisher Scientific, eBioscience, or BioLegend: CD3 (145-2C11), CD4 (RM4-5), CD8 (53-6.7), B220 (RA3-6B2), CD11b (M1/70), CD11c (N418), MHC II (I-A/I-E; M5/114.15.2), Ly6G (1A8), Ly6C (HK1.4), CD115 (AFS98), F4/80 (BM8), NK1.1 (PK136), and CD27 (LG.3A10). Cell types were defined as follows: T cells ($CD3^+$), CD4 T cells ($CD3^+$ $CD4^+$), CD8 T cells ($CD3^+$ $CD8^+$), B cells ($CD3^-$ $B220^+$), DCs ($CD3^-$ $B220^-$ $Ly6G^-$ $CD115^-$ MHC II^+ $CD11c^+$), $CD8^+$ cDCs ($CD3^-$ $B220^-$ $Ly6G^-$ $CD115^-$ MHC II^+ $CD11c^+$ $CD8^+$), $CD11b^+$ cDCs ($CD3^-$ $B220^-$ $Ly6G^-$ $CD115^-$ MHC II^+ $CD11c^+$ $CD11b^+$), macrophages ($CD3^-$ $B220^-$ $Ly6G^-$ $CD115^-$ $CD11c^-$ $CD11b^-$ $F4/80^+$), and NK cells ($CD3^-$ $B220^-$ $Ly6G^-$ $CD115^-$ $CD11c^-$ $F4/80^-$ $NK1.1^+$ $CD11b^{hi/lo}$ $CD27^{hi/lo}$). In addition, monocytes were gated as previously described ($CD3^-$ $B220^-$ $Ly6G^-$ $NK1.1^-$ $CD115^+$ $CD11b^+$; Hanna et al., 2011). $CD115^+$ and $CD11b^+$ cells were then grouped based on their expression of Ly6C ($Ly6C^{hi}$ and $Ly6C^{lo}$ monocytes). Fluorescence minus one controls were used to define populations positively stained with anti-Ly6G, -Ly6C, -CD115, and -NK1.1 antibodies. Data were acquired using a flow cytometer (LSRII; BD) and FACS Diva software (version 8.0) and analyzed using FlowJo (8.8.7; Tree Star). The flow cytometric gating strategy can be found in Fig. S1.

Histology and immunohistochemistry

After euthanasia with CO_2, tissues (brain, liver, kidney, spleen, pancreas, heart, lungs, spinal cord, and bone marrow) from uninfected *Irf2*$^{-/-}$ and WT mice and moribund SVN-infected *Irf2*$^{-/-}$ and age-matched WT mice 6–7 d after infection were collected and fixed by immersion in 10% neutral buffered formalin for 48 h, processed in ethanol and xylene, embedded in paraffin, sectioned at 5-µm thickness, stained with H&E, and examined by a board-certified veterinary pathologist (S. Monette). To identify the small percentage of infected WT mice with positive brain viral titers, the left halves of the brains were harvested on day 5 p.i. and fixed in neutral buffered formalin, whereas the right halves were homogenized, and supernatant was collected for RNA extraction to determine SVN RNA copy number by SINV TaqMan RT-qPCR. Then, the brain samples with positive viral RNA levels were processed and embedded in paraffin for histological examination. For histological analysis of inflammation, sections were stained with H&E and antibodies for specific immune cell markers and were scored in a blinded fashion using a scale of zero to four as follows: 1, minimal; 2, mild; 3, moderate; and 4, severe.

Tissues were stained by immunohistochemistry for CD3 (primary antibody VP-RM01 [Vector Laboratories] applied at a concentration of 1:100 after heat-induced epitope retrieval [HIER] in a buffer, pH 9.0), B220 (550286; BD; 1:200, HIER, pH 6.0), Mac-2 (CL8942B; Cedarlane; 1:100; HIER, pH 6.0), granzyme B (ab4059; Abcam; 1:250; HIER, pH 6.0), cleaved caspase-3 (9661; Cell Signaling Technology; 1:250; HIER, pH 6.0), and SINV capsid (rabbit polyclonal; Rice and Strauss, 1982; 1:10,000, HIER, pH 6.0). Mac-2 and SINV capsid staining was performed manually with an avidin-biotin detection system (Vectastain ABC Elite kit; PK-6100; Vector Laboratories). Other stains were performed on an automated stainer (Bond RX; Leica Biosystems) using the Bond Polymer Refine detection kit (DS9800; Leica Biosystems). With both manual and automated methods, the positive signal was labeled with 3,3′-Diaminobenzidine (DAB), and sections were counterstained with hematoxylin. Sections were also stained by the TUNEL method as previously described (Gavrieli et al., 1992). All H&E, immunohistochemistry, and TUNEL slides were examined by a board-certified veterinary pathologist (S. Monette).

Images were acquired using a microscope (BX45; Olympus) using a 20× objective, a DP25 camera, and cellSens Entry software (1.9; Olympus). For each stain in each animal, eight images measuring each 567,162 μm^2 were acquired from defined regions of interest as shown in Fig. S2. Images were then analyzed using ImageJ software (1.49; National Institutes of Health) with the Color Deconvolution plugin (1.5; Ruifrok and Johnston, 2001) to determine the staining area. After deconvolution with the H DAB vector, the Threshold tool (lower and upper values set at 0 and 150 [B220 stain] or 170 [SINV capsid stain], respectively) was applied to the DAB component to produce a black and white image. The Measure tool was used to determine the percentage of positive (black) pixels (positive staining area). The number of positive cells was also counted manually from the same images.

In vivo blocking antibody treatment and immune cell depletion

WT and *Irf2*$^{-/-}$ mice were treated i.p. with anti-IFNAR1 antibody (clone MAR1-5A3; Sheehan et al., 2006) before SVN infection on day −1 (500 µg or 1 mg) or on day 2 p.i. (500 µg) or with mouse IgG1 isotype control (clone MOPC21; Bio X Cell) on day −1 before virus infection. In some experiments, WT mice were depleted of NK cells with anti-NK1.1 antibody (clone PK136; Bio X Cell) or treated with mouse IgG2a isotype control (clone C1.18.4.; Bio X Cell) 1 d before infection (300 µg). For MNP depletion, WT and *Irf2*$^{-/-}$ mice were treated i.p. with 200 µl clodronate or PBS liposome on day −3 before SVN infection.

Adoptive transfer of B cell and serum

For B cell adoptive transfer, whole spleens from WT mice were harvested, and single-cell suspensions of splenocytes were obtained, from which B cells (CD19$^+$) were isolated by negative selection using magnetic particles bound to a cocktail of antibodies recognizing non–B cells according to the manufacturer's protocol (STEMCELL Technologies). CD19$^+$ enriched cells from each of the WT mice were counted, and 2×10^6 cells from each animal were pooled together for i.p. injection into naive WT and *Irf2*$^{-/-}$ mice 1 d before SVN infection (2×10^6 cells per injection). For serum transfer, WT mice were infected with SVN, and serum was harvested on day 7 p.i. Samples were heat inactivated at 56°C for 30 min and pooled together for later injection. Naive WT and *Irf2*$^{-/-}$ mice were infected with SVN and 1 d later treated i.p. with 200 µl of serum.

Plaque reduction neutralization test (PRNT)

Serum samples from uninfected mice diluted 1:100 were incubated with different concentrations of SVN. After incubation at 37°C for 1 h, 200 µl of the mixture (200 µl serum dilution + 200 µl virus dilution) was inoculated onto a monolayer of BHK-21 cells in 6-well plates using a final 2.25% avicel overlay, and 30 h p.i., the cells were visualized with crystal violet staining. The concentration of virus that gave ∼200 plaques per well was chosen for the subsequent PRNT. Serum samples from day 5 SVN-infected WT and *Irf2*$^{-/-}$ mice initially diluted 1:100 were then serially diluted threefold and mixed with a constant concentration of virus.

Statistical analyses

Survival was compared using Kaplan-Meier survival curves (log-rank test). Differences between groups during the course of infection were determined using two-way ANOVA and Bonferroni posttests. Differences between groups at a single time point were determined using an unpaired, two-tailed Student's *t* test with a 95% confidence interval. All statistical analyses were done using Prism 5 (GraphPad Software).

Online supplemental material

Fig. S1 shows the FACS gating strategy for defining T cell, B cell, DC, macrophage, NK cell, and monocyte populations in the mouse spleen. Fig. S2 shows the eight different locations in the brain from which images of SVN-infected WT and *Irf2*$^{-/-}$ mice were taken for quantification of B cell staining. Table S1 shows the sequences of primers used for ISG and SINV TaqMan RT-qPCR.

ACKNOWLEDGMENTS

We thank the University Health Network (Toronto, Canada) and Tak Wah Mak (University of Toronto, Canada) for *Irf2*$^{+/-}$ mice; Juana Gonzalez for assistance on flow cytometry; Meike Dittmann for the primers for ISG RT-qPCR; Hachung Chung for the primers for SINV TaqMan RT-qPCR; Corrine Quirk for mouse colony maintenance; Kai-Hui Yao for assistance with retroorbital injections; and Ursula Andreo, Hachung Chung, and Bill Schneider for critical reading of the manuscript.

This work was supported in part by a Career Development Fellowship from Northeast Biodefense Center/Columbia University (Lipkin; 5 U54 AI057158-09), a Memorial Sloan-Kettering Cancer Center Support Grant from the National Institutes of Health (P30 CA008748), a National Institutes of Health grant (AI091707), the Starr Foundation, the Greenberg Medical Research Institute, and anonymous donors. The use of the BD LSRII flow cytometer and FLUOstar Omega Plate reader was supported by a grant from

the National Center for Advancing Translational Sciences (UL1 TR000043) and the National Institutes of Health Clinical and Translational Science Award program.

The authors declare no competing financial interests.

Submitted: 24 February 2016
Revised: 9 September 2016
Accepted: 1 November 2016

REFERENCES

Auffray, C., D.K. Fogg, E. Narni-Mancinelli, B. Senechal, C. Trouillet, N. Saederup, J. Leemput, K. Bigot, L. Campisi, M. Abitbol, et al. 2009. CX_3CR1^+ $CD115^+$ $CD135^+$ common macrophage/DC precursors and the role of CX_3CR1 in their response to inflammation. *J. Exp. Med.* 206:595–606. http://dx.doi.org/10.1084/jem.20081385

Baccala, R., M.J. Welch, R. Gonzalez-Quintial, K.B. Walsh, J.R. Teijaro, A. Nguyen, C.T. Ng, B.M. Sullivan, A. Zarpellon, Z.M. Ruggeri, et al. 2014. Type I interferon is a therapeutic target for virus-induced lethal vascular damage. *Proc. Natl. Acad. Sci. USA.* 111:8925–8930. http://dx.doi.org/10.1073/pnas.1408148111

Bick, M.J., J.W. Carroll, G. Gao, S.P. Goff, C.M. Rice, and M.R. MacDonald. 2003. Expression of the zinc-finger antiviral protein inhibits alphavirus replication. *J. Virol.* 77:11555–11562. http://dx.doi.org/10.1128/JVI.77.21.11555-11562.2003

Brennan, K., and A.G. Bowie. 2010. Activation of host pattern recognition receptors by viruses. *Curr. Opin. Microbiol.* 13:503–507. http://dx.doi.org/10.1016/j.mib.2010.05.007

Chiossone, L., J. Chaix, N. Fuseri, C. Roth, E. Vivier, and T. Walzer. 2009. Maturation of mouse NK cells is a 4-stage developmental program. *Blood.* 113:5488–5496. http://dx.doi.org/10.1182/blood-2008-10-187179

Chow, A., B.D. Brown, and M. Merad. 2011. Studying the mononuclear phagocyte system in the molecular age. *Nat. Rev. Immunol.* 11:788–798. http://dx.doi.org/10.1038/nri3087

Dubuisson, J., S. Lustig, N. Ruggli, Y. Akov, and C.M. Rice. 1997. Genetic determinants of Sindbis virus neuroinvasiveness. *J. Virol.* 71:2636–2646.

Fairfax, B.P., P. Humburg, S. Makino, V. Naranbhai, D. Wong, E. Lau, L. Jostins, K. Plant, R. Andrews, C. McGee, and J.C. Knight. 2014. Innate immune activity conditions the effect of regulatory variants upon monocyte gene expression. *Science.* 343:1246949. http://dx.doi.org/10.1126/science.1246949

Gao, P.S., D.Y. Leung, N.M. Rafaels, M. Boguniewicz, T. Hand, L. Gao, T.R. Hata, L.C. Schneider, J.M. Hanifin, T.H. Beaty, et al. 2012. Genetic variants in interferon regulatory factor 2 (IRF2) are associated with atopic dermatitis and eczema herpeticum. *J. Invest. Dermatol.* 132:650–657. http://dx.doi.org/10.1038/jid.2011.374

Gardner, C.L., C.W. Burke, M.Z. Tesfay, P.J. Glass, W.B. Klimstra, and K.D. Ryman. 2008. Eastern and Venezuelan equine encephalitis viruses differ in their ability to infect dendritic cells and macrophages: impact of altered cell tropism on pathogenesis. *J. Virol.* 82:10634–10646. http://dx.doi.org/10.1128/JVI.01323-08

Gardner, J.P., I. Frolov, S. Perri, Y. Ji, M.L. MacKichan, J. zur Megede, M. Chen, B.A. Belli, D.A. Driver, S. Sherrill, et al. 2000. Infection of human dendritic cells by a sindbis virus replicon vector is determined by a single amino acid substitution in the E2 glycoprotein. *J. Virol.* 74:11849–11857. http://dx.doi.org/10.1128/JVI.74.24.11849-11857.2000

Gavrieli, Y., Y. Sherman, and S.A. Ben-Sasson. 1992. Identification of programmed cell death in situ via specific labeling of nuclear DNA fragmentation. *J. Cell Biol.* 119:493–501. http://dx.doi.org/10.1083/jcb.119.3.493

Grieder, F.B., and S.N. Vogel. 1999. Role of interferon and interferon regulatory factors in early protection against Venezuelan equine encephalitis virus infection. *Virology.* 257:106–118. http://dx.doi.org/10.1006/viro.1999.9662

Griffin, D.E., and J.L. Hess. 1986. Cells with natural killer activity in the cerebrospinal fluid of normal mice and athymic nude mice with acute Sindbis virus encephalitis. *J. Immunol.* 136:1841–1845.

Guan, J., S.M.S. Miah, Z.S. Wilson, T.K. Erick, C. Banh, and L. Brossay. 2014. Role of type I interferon receptor signaling on NK cell development and functions. *PLoS One.* 9:e111302. http://dx.doi.org/10.1371/journal.pone.0111302

Hanna, R.N., L.M. Carlin, H.G. Hubbeling, D. Nackiewicz, A.M. Green, J.A. Punt, F. Geissmann, and C.C. Hedrick. 2011. The transcription factor NR4A1 (Nur77) controls bone marrow differentiation and the survival of $Ly6C^-$ monocytes. *Nat. Immunol.* 12:778–785. http://dx.doi.org/10.1038/ni.2063

Harada, H., T. Fujita, M. Miyamoto, Y. Kimura, M. Maruyama, A. Furia, T. Miyata, and T. Taniguchi. 1989. Structurally similar but functionally distinct factors, IRF-1 and IRF-2, bind to the same regulatory elements of IFN and IFN-inducible genes. *Cell.* 58:729–739. http://dx.doi.org/10.1016/0092-8674(89)90107-4

Hastie, E., M. Cataldi, I. Marriott, and V.Z. Grdzelishvili. 2013. Understanding and altering cell tropism of vesicular stomatitis virus. *Virus Res.* 176:16–32. http://dx.doi.org/10.1016/j.virusres.2013.06.003

Haynes, L.D., S. Verma, B. McDonald, R. Wu, R. Tacke, H.N. Nowyhed, J. Ekstein, A. Feuvrier, C.A. Benedict, and C.C. Hedrick. 2015. Cardif (MAVS) regulates the maturation of NK cells. *J. Immunol.* 195:2157–2167. http://dx.doi.org/10.4049/jimmunol.1402060

Hida, S., K. Ogasawara, K. Sato, M. Abe, H. Takayanagi, T. Yokochi, T. Sato, S. Hirose, T. Shirai, S. Taki, and T. Taniguchi. 2000. $CD8^+$ T cell–mediated skin disease in mice lacking IRF-2, the transcriptional attenuator of interferon-α/β signaling. *Immunity.* 13:643–655. http://dx.doi.org/10.1016/S1074-7613(00)00064-9

Hirsch, R.L. 1981. Natural killer cells appear to play no role in the recovery of mice from Sindbis virus infection. *Immunology.* 43:81–89.

Hochweller, K., J. Striegler, G.J. Hämmerling, and N. Garbi. 2008. A novel CD11c.DTR transgenic mouse for depletion of dendritic cells reveals their requirement for homeostatic proliferation of natural killer cells. *Eur. J. Immunol.* 38:2776–2783. http://dx.doi.org/10.1002/eji.200838659

Honda, K., and T. Taniguchi. 2006. IRFs: master regulators of signalling by Toll-like receptors and cytosolic pattern-recognition receptors. *Nat. Rev. Immunol.* 6:644–658. http://dx.doi.org/10.1038/nri1900

Honda, K., T. Mizutani, and T. Taniguchi. 2004. Negative regulation of IFN-α/β signaling by IFN regulatory factor 2 for homeostatic development of dendritic cells. *Proc. Natl. Acad. Sci. USA.* 101:2416–2421. http://dx.doi.org/10.1073/pnas.0307336101

Ichikawa, E., S. Hida, Y. Omatsu, S. Shimoyama, K. Takahara, S. Miyagawa, K. Inaba, and S. Taki. 2004. Defective development of splenic and epidermal $CD4^+$ dendritic cells in mice deficient for IFN regulatory factor-2. *Proc. Natl. Acad. Sci. USA.* 101:3909–3914. http://dx.doi.org/10.1073/pnas.0400610101

Iijima, N., and A. Iwasaki. 2016. Access of protective antiviral antibody to neuronal tissues requires CD4 T-cell help. *Nature.* 533:552–556. http://dx.doi.org/10.1038/nature17979

Jackson, A.C., T.R. Moench, D.E. Griffin, and R.T. Johnson. 1987. The pathogenesis of spinal cord involvement in the encephalomyelitis of mice caused by neuroadapted Sindbis virus infection. *Lab. Invest.* 56:418–423.

Jackson, A.C., T.R. Moench, B.D. Trapp, and D.E. Griffin. 1988. Basis of neurovirulence in Sindbis virus encephalomyelitis of mice. *Lab. Invest.* 58:503–509.

Karki, S., M.M.H. Li, J.W. Schoggins, S. Tian, C.M. Rice, and M.R. MacDonald. 2012. Multiple interferon stimulated genes synergize with the zinc finger antiviral protein to mediate anti-alphavirus activity. *PLoS One.* 7:e37398. http://dx.doi.org/10.1371/journal.pone.0037398

Klimstra, W.B., K.D. Ryman, K.A. Bernard, K.B. Nguyen, C.A. Biron, and R.E. Johnston. 1999. Infection of neonatal mice with sindbis virus results in a systemic inflammatory response syndrome. *J. Virol.* 73:10387–10398.

Kulcsar, K.A., V.K. Baxter, R. Abraham, A. Nelson, and D.E. Griffin. 2015. Distinct immune responses in resistant and susceptible strains of mice during neurovirulent alphavirus encephalomyelitis. *J. Virol.* 89:8280–8291. http://dx.doi.org/10.1128/JVI.00173-15

Levine, B., J.M. Hardwick, B.D. Trapp, T.O. Crawford, R.C. Bollinger, and D.E. Griffin. 1991. Antibody-mediated clearance of alphavirus infection from neurons. *Science.* 254:856–860. http://dx.doi.org/10.1126/science.1658936

Li, H.S., A. Gelbard, G.J. Martinez, E. Esashi, H. Zhang, H. Nguyen-Jackson, Y.-J. Liu, W.W. Overwijk, and S.S. Watowich. 2011. Cell-intrinsic role for IFN-α-STAT1 signals in regulating murine Peyer patch plasmacytoid dendritic cells and conditioning an inflammatory response. *Blood.* 118:3879–3889. http://dx.doi.org/10.1182/blood-2011-04-349761

Lohoff, M., G.S. Duncan, D. Ferrick, H.W. Mittrücker, S. Bischof, S. Prechtl, M. Röllinghoff, E. Schmitt, A. Pahl, and T.W. Mak. 2000. Deficiency in the transcription factor interferon regulatory factor (IRF)-2 leads to severely compromised development of natural killer and T helper type 1 cells. *J. Exp. Med.* 192:325–336. http://dx.doi.org/10.1084/jem.192.3.325

Lucas, M., W. Schachterle, K. Oberle, P. Aichele, and A. Diefenbach. 2007. Dendritic cells prime natural killer cells by trans-presenting interleukin 15. *Immunity.* 26:503–517. http://dx.doi.org/10.1016/j.immuni.2007.03.006

Lustig, S., A.C. Jackson, C.S. Hahn, D.E. Griffin, E.G. Strauss, and J.H. Strauss. 1988. Molecular basis of Sindbis virus neurovirulence in mice. *J. Virol.* 62:2329–2336.

Lustig, S., M. Halevy, D. Ben-Nathan, and Y. Akov. 1992. A novel variant of Sindbis virus is both neurovirulent and neuroinvasive in adult mice. *Arch. Virol.* 122:237–248. http://dx.doi.org/10.1007/BF01317186

Madera, S., M. Rapp, M.A. Firth, J.N. Beilke, L.L. Lanier, and J.C. Sun. 2016. Type I IFN promotes NK cell expansion during viral infection by protecting NK cells against fratricide. *J. Exp. Med.* 213:225–233. http://dx.doi.org/10.1084/jem.20150712

Matsuyama, T., T. Kimura, M. Kitagawa, K. Pfeffer, T. Kawakami, N. Watanabe, T.M. Kündig, R. Amakawa, K. Kishihara, A. Wakeham, et al. 1993. Targeted disruption of IRF-1 or IRF-2 results in abnormal type I IFN gene induction and aberrant lymphocyte development. *Cell.* 75:83–97. http://dx.doi.org/10.1016/S0092-8674(05)80086-8

Metcalf, T.U., V.K. Baxter, V. Nilaratanakul, and D.E. Griffin. 2013. Recruitment and retention of B cells in the central nervous system in response to alphavirus encephalomyelitis. *J. Virol.* 87:2420–2429. http://dx.doi.org/10.1128/JVI.01769-12

Minamino, K., K. Takahara, T. Adachi, K. Nagaoka, T. Iyoda, S. Taki, and K. Inaba. 2012. IRF-2 regulates B-cell proliferation and antibody production through distinct mechanisms. *Int. Immunol.* 24:573–581. http://dx.doi.org/10.1093/intimm/dxs060

Pialoux, G., B.A. Gaüzère, S. Jauréguiberry, and M. Strobel. 2007. Chikungunya, an epidemic arbovirosis. *Lancet Infect. Dis.* 7:319–327. http://dx.doi.org/10.1016/S1473-3099(07)70107-X

Powers, A.M., and C.H. Logue. 2007. Changing patterns of chikungunya virus: re-emergence of a zoonotic arbovirus. *J. Gen. Virol.* 88:2363–2377. http://dx.doi.org/10.1099/vir.0.82858-0

Rhodehouse, B.C., J.N. Mayo, R.S. Beard Jr., C.H. Chen, and S.E. Bearden. 2013. Opening of the blood-brain barrier before cerebral pathology in mild hyperhomocysteinemia. *PLoS One.* 8:e63951. http://dx.doi.org/10.1371/journal.pone.0063951

Rice, C.M., and J.H. Strauss. 1982. Association of sindbis virion glycoproteins and their precursors. *J. Mol. Biol.* 154:325–348. http://dx.doi.org/10.1016/0022-2836(82)90067-5

Ruifrok, A.C., and D.A. Johnston. 2001. Quantification of histochemical staining by color deconvolution. *Anal. Quant. Cytol. Histol.* 23:291–299.

Ryman, K.D., and W.B. Klimstra. 2008. Host responses to alphavirus infection. *Immunol. Rev.* 225:27–45. http://dx.doi.org/10.1111/j.1600-065X.2008.00670.x

Ryman, K.D., W.B. Klimstra, K.B. Nguyen, C.A. Biron, and R.E. Johnston. 2000. Alpha/beta interferon protects adult mice from fatal Sindbis virus infection and is an important determinant of cell and tissue tropism. *J. Virol.* 74:3366–3378. http://dx.doi.org/10.1128/JVI.74.7.3366-3378.2000

Ryman, K.D., K.C. Meier, C.L. Gardner, P.A. Adegboyega, and W.B. Klimstra. 2007. Non-pathogenic Sindbis virus causes hemorrhagic fever in the absence of alpha/beta and gamma interferons. *Virology.* 368:273–285. http://dx.doi.org/10.1016/j.virol.2007.06.039

Salkowski, C.A., S.A. Barber, G.R. Detore, and S.N. Vogel. 1996. Differential dysregulation of nitric oxide production in macrophages with targeted disruptions in IFN regulatory factor-1 and -2 genes. *J. Immunol.* 156:3107–3110.

Sato, T., N. Onai, H. Yoshihara, F. Arai, T. Suda, and T. Ohteki. 2009. Interferon regulatory factor-2 protects quiescent hematopoietic stem cells from type I interferon-dependent exhaustion. *Nat. Med.* 15:696–700. http://dx.doi.org/10.1038/nm.1973

Schneider, W.M., M.D. Chevillotte, and C.M. Rice. 2014. Interferon-stimulated genes: a complex web of host defenses. *Annu. Rev. Immunol.* 32:513–545. http://dx.doi.org/10.1146/annurev-immunol-032713-120231

Schoggins, J.W., S.J. Wilson, M. Panis, M.Y. Murphy, C.T. Jones, P. Bieniasz, and C.M. Rice. 2011. A diverse range of gene products are effectors of the type I interferon antiviral response. *Nature.* 472:481–485. http://dx.doi.org/10.1038/nature09907

Schoggins, J.W., D.A. MacDuff, N. Imanaka, M.D. Gainey, B. Shrestha, J.L. Eitson, K.B. Mar, R.B. Richardson, A.V. Ratushny, V. Litvak, et al. 2014. Pan-viral specificity of IFN-induced genes reveals new roles for cGAS in innate immunity. *Nature.* 505:691–695. http://dx.doi.org/10.1038/nature12862

Schreiber, H.A., J. Loschko, R.A. Karssemeijer, A. Escolano, M.M. Meredith, D. Mucida, P. Guermonprez, and M.C. Nussenzweig. 2013. Intestinal monocytes and macrophages are required for T cell polarization in response to *Citrobacter rodentium*. *J. Exp. Med.* 210:2025–2039. http://dx.doi.org/10.1084/jem.20130903

Schuffenecker, I., I. Iteman, A. Michault, S. Murri, L. Frangeul, M.C. Vaney, R. Lavenir, N. Pardigon, J.M. Reynes, F. Pettinelli, et al. 2006. Genome microevolution of chikungunya viruses causing the Indian Ocean outbreak. *PLoS Med.* 3:e263. http://dx.doi.org/10.1371/journal.pmed.0030263

Sheehan, K.C.F., K.S. Lai, G.P. Dunn, A.T. Bruce, M.S. Diamond, J.D. Heutel, C. Dungo-Arthur, J.A. Carrero, J.M. White, P.J. Hertzog, and R.D. Schreiber. 2006. Blocking monoclonal antibodies specific for mouse IFN-α/β receptor subunit 1 (IFNAR-1) from mice immunized by in vivo hydrodynamic transfection. *J. Interferon Cytokine Res.* 26:804–819. http://dx.doi.org/10.1089/jir.2006.26.804

Sherman, L.A., and D.E. Griffin. 1990. Pathogenesis of encephalitis induced in newborn mice by virulent and avirulent strains of Sindbis virus. *J. Virol.* 64:2041–2046.

Shi, C., and E.G. Pamer. 2011. Monocyte recruitment during infection and inflammation. *Nat. Rev. Immunol.* 11:762–774. http://dx.doi.org/10.1038/nri3070

Taki, S. 2002. Type I interferons and autoimmunity: lessons from the clinic and from IRF-2-deficient mice. *Cytokine Growth Factor Rev.* 13:379–391. http://dx.doi.org/10.1016/S1359-6101(02)00023-0

Taki, S., S. Nakajima, E. Ichikawa, T. Saito, and S. Hida. 2005. IFN regulatory factor-2 deficiency revealed a novel checkpoint critical for the generation of peripheral NK cells. *J. Immunol.* 174:6005–6012. http://dx.doi.org/10.4049/jimmunol.174.10.6005

Teijaro, J.R., C. Ng, A.M. Lee, B.M. Sullivan, K.C. Sheehan, M. Welch, R.D. Schreiber, J.C. de la Torre, and M.B. Oldstone. 2013. Persistent LCMV infection is controlled by blockade of type I interferon signaling. *Science.* 340:207–211. http://dx.doi.org/10.1126/science.1235214

Trgovcich, J., J.F. Aronson, and R.E. Johnston. 1996. Fatal Sindbis virus infection of neonatal mice in the absence of encephalitis. *Virology.* 224:73–83. http://dx.doi.org/10.1006/viro.1996.0508

Trgovcich, J., J.F. Aronson, J.C. Eldridge, and R.E. Johnston. 1999. TNFα, interferon, and stress response induction as a function of age-related susceptibility to fatal Sindbis virus infection of mice. *Virology.* 263:339–348. http://dx.doi.org/10.1006/viro.1999.9913

Varol, C., L. Landsman, D.K. Fogg, L. Greenshtein, B. Gildor, R. Margalit, V. Kalchenko, F. Geissmann, and S. Jung. 2007. Monocytes give rise to mucosal, but not splenic, conventional dendritic cells. *J. Exp. Med.* 204:171–180. http://dx.doi.org/10.1084/jem.20061011

Wang, T., T. Town, L. Alexopoulou, J.F. Anderson, E. Fikrig, and R.A. Flavell. 2004. Toll-like receptor 3 mediates West Nile virus entry into the brain causing lethal encephalitis. *Nat. Med.* 10:1366–1373. http://dx.doi.org/10.1038/nm1140

Wilson, E.B., D.H. Yamada, H. Elsaesser, J. Herskovitz, J. Deng, G. Cheng, B.J. Aronow, C.L. Karp, and D.G. Brooks. 2013. Blockade of chronic type I interferon signaling to control persistent LCMV infection. *Science.* 340:202–207. http://dx.doi.org/10.1126/science.1235208